THE JOURNAL OF PHYSICAL CHEMISTRY B

ARTICLE

pubs.acs.org/JPCB

Radiation and Radical Chemistry of NO_3^-, HNO_3, and Dialkylphosphoric Acids in Room-Temperature Ionic Liquids

Ilya A. Shkrob,*[,†] Timothy W. Marin,[†,‡] S. D. Chemerisov,[†] and J. F. Wishart[§]

[†]Chemical Sciences and Engineering Division, Argonne National Laboratory, 9700 South Cass Avenue, Argonne, Illinois 60439, United States

[‡]Chemistry Department, Benedictine University, 5700 College Road, Lisle, Illinois 60532, United States

[§]Chemistry Department, Brookhaven National Laboratory, Upton, New York 11973-5000, United States

Supporting Information

ABSTRACT: Hydrophobic room-temperature ionic liquids (ILs) are considered as possible replacements for molecular diluents for nuclear separations, as well as the basis of new separations processes. Such applications may put the solvents both in high radiation fields and in contact with aqueous raffinate containing 1−6 M HNO_3. In this study, we address the effect of the extracted nitrate and nitric acid on the radiation chemistry of hydrophobic ILs composed of 1-alkyl-3-methylimidazolium cations (and closely related systems). We demonstrate that the nitrate anion competes with the solvent cation as an electron scavenger, with most of the primary radical species converted to $NO_3^{\bullet 2-}$ and $NO_2^{\bullet}$ that initiate a complex sequence of radical reactions. In hydrophobic ILs equilibrated with 3 M HNO_3, nearly all electrons released by the ionizing radiation are converted to $NO_2^{\bullet}$. While the reductive pathway is strongly affected by the nitrate and there is also some N−O bond scission via direct excitation, the extent of interference with the oxidative pathway is relatively small; the cation damage is not dramatically affected by the presence of nitrate as most of the detrimental radiolytic products are generated via the oxidative pathway. These results are contrasted with the behavior of dialkylphosphoric acids (a large class of extraction agents for trivalent metal ions). We demonstrate that IL solvents protect these dialkylphosphoric acids against radiation-induced dealkylation.

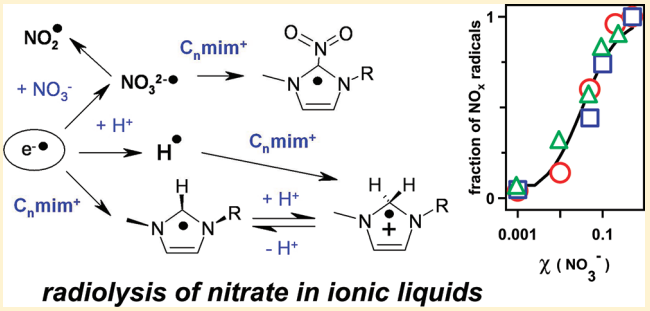

1. INTRODUCTION

Hydrophobic room-temperature ionic liquids (ILs)[1] exhibit several properties (such as low volatility, electric conductivity, and excellent solvation of metal ions) that make them an attractive choice as diluents in liquid−liquid extraction of radionuclide ions to replace more common molecular diluents used in "wet" processing of spent nuclear fuel.[2−6] In such separations, the aqueous raffinate containing radionuclide ions (such as UO_2^{2+}, Pu^{IV}, trivalent lanthanide ions and minor actinides, TcO_4^-, platinum group ions, Cs^+, and Sr^{2+}, etc.) is strongly acidic, containing 1−8 M HNO_3. This nitric acid is introduced during the dissolution of the fuel rods, and high acidity is maintained during the separations, for two reasons. First, the high acidity prevents hydrolysis of some of the metal ions (for example, Pu^{IV} readily hydrolyzes at pH > 1, forming colloidal particles). Second, many of the ion-specific extracting agents and ionophores are *neutral* molecules, and the metal complexes that are extracted into the organic phase involve the anions present in the raffinate. The nitrate serves both to charge neutralize the extracted complex and coordinate in the first shell of the extracted metal complexes, so a large nitrate concentration is required to shift the extraction equilibria. Even for ionophores (such as crown ethers) that form complexes with Cs^+ and Sr^{2+} and only loosely associate with the anion, the replacement of the nitrate with other anions dramatically reduces the extraction efficacy because other anions are less efficiently solvated by organic diluents, resulting in the thermodynamic and kinetic barriers counteracting interfacial transport.[7,8] Thus, except for some special situations (such as the separations of the trivalent ions using dialkylphosphoric acids in the organic phase and polyaminocarboxylic acids in the aqueous phase),[9] metal extraction typically involves contact of the organic diluent (containing the extraction agents) with 1−8 M nitric acid solutions.

Our nuclear magnetic resonance (NMR) studies[8] as well as data obtained in other laboratories[10,11] demonstrate that even highly hydrophobic ILs efficiently extract water and nitric acid from such aqueous solutions. The concentration of the extracted nitric acid compares to that in mildly polar molecular solvents, such as 1-octanol.[8,10] Some of this extraction proceeds via ion exchange (the exchange of protons and constituting cations of the IL across the interface), but most of it involves the extraction of either dissociated and associated HNO_3.[8] Thus, the typical IL

Received: July 11, 2011
Revised: August 2, 2011
Published: August 08, 2011

Scheme 1. 1-Alkyl-3-methylimidazolium Cations and Radical Intermediates Derived from Such Cations in Radiolysis of the Corresponding ILs

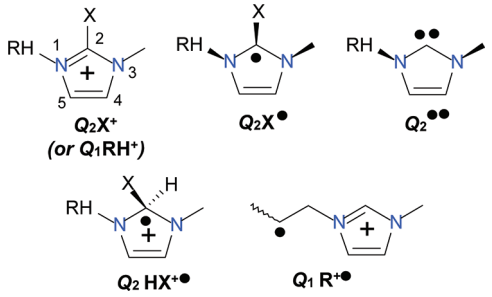

solvent equilibrated with the aqueous raffinate contains 5−15 mol % nitrate. Given this extensive extraction, the physicochemical properties of such IL solvents are significantly different from neat ILs. In this study we examine how the uptake of nitrate and nitric acid changes the radiation chemistry of the ILs.

In the course of radionuclide extraction, the IL solvent is exposed to strong ionizing radiation generated by the decaying radioisotopes. For neat ILs, the mechanistic aspects of this chemistry have been addressed in a series of studies from our two laboratories,[7,12−16] and these structural studies have been complemented by pulse radiolysis−transient absorption spectroscopy (e.g., see refs 17−20) and product analyses studies (e.g., see refs 21−26) by other groups. However, it is important to understand the effects of radiation on ILs when they are equilibrated with aqueous HNO_3 raffinate (as discussed above) in order to close the gap that exists between the work done so far on neat ILs (and IL solutions) and the complexity of the extraction systems in use today. To our knowledge, there has only been a single study to date of the effect of nitric acid on IL radiolysis,[22] in which increasing HNO_3 concentrations strongly inhibited the accumulation of colored radiolysis products, but no reaction intermediates or products were identified. The goal of this study is to elucidate the radiolytic reaction mechanisms and intermediates of IL−nitric acid mixtures. Specifically, we demonstrate that the radiation chemistry of IL solvents in contact with raffinate solutions changes very significantly as compared to neat ILs, and this raises awareness that the previous work on irradiated ILs and IL−solute mixtures is only the first step in the assessment of the behavior of IL-based extraction systems in the presence of radiation.

For practical considerations, we limited our study to ILs composed of 1-alkyl-3-methylimidazolium cations ($C_n$mim$^+$; Scheme 1), as such liquids presently comprise the largest class of chemically stable ILs that are explored in nuclear separations. Depending on the hydrophobicity of the constituent ions, it is possible to obtain water-miscible (nitrate, acetate, and triflate (TfO^-)) or less miscible (BF_4^-, PF_6^-, bistriflimide (NTf_2^-)) ionic liquids composed of these imidazolium cations. If the alkyl chain in the cation is sufficiently long ($n > 6$), the exchange of the hydronium ion present in the aqueous solution with $C_n$mim$^+$ in the IL phase becomes negligible,[8] and the extraction of the nitric acid is neutral (rather than by ion exchange). Importantly, even these (nominally, "hydrophobic") ILs, such as $C_n$mimNTf_2 (n = 8, 10) contain 10−15 mol % of water after equilibration with aqueous solutions.[8]

Because nitric acid is a particular example of a *Brönsted acid*, the second question we address in the present study is the general effect of acidity on the radiation chemistry of ILs. One class of such acids, dialkylphosphoric acids ($HO_2P(OR)_2$), is of particular interest for separations chemistry, as such ligands are used to extract trivalent ions, such as lanthanides and Am^{3+} and Cm^{3+}. The typical extracting agent of this type is bis (2-ethylhexyl)phosphoric acid (HDEHP).[27] In solution, two HDEHP molecules form a ∼P═O···HO−P∼ bound dimer and three of these dimers (after deprotonation of the ligands) form a cage around the Ln^{3+} ions, with each HDEHP···DEHP$^-$ unit chelating the metal ion in a bidentate fashion. The resulting complex exhibits exceptional ionic radius selectivity, and this property is used in many practically important separations schemes (e.g., the DIAMEX-SANEX process)[28] but most importantly in the TALSPEAK process,[27] in which the competition between the chelation of the metal ions by HDEHP in an organic diluent and polyaminocarboxylic acids (that are also ionic-radius-selecting) in the aqueous phase is used to separate the lanthanides from minor actinides. Currently, IL-based separations involving dialkylphosphoric acid extractants are being vigorously pursued by several groups.[29] Because the polyaminocarboxylic acids must be ionized for complexation, such separations involve aqueous solutions containing low (<0.1 M) nitrate concentrations.[28,29] However, the concentration of dialkylphosphoric acid in the organic diluent is 0.1−1 M. Thus, once again the question arises whether the presence of so much acid in the IL affects its radiation chemistry. The related concern, in this case, is the radiation damage to the extractant, as it is known from previous studies (see the recent review in ref 9) that the irradiation of neat and diluted dialkylphosphoric acid results in efficient dealkylation of the extractant with the formation of (less specifically binding) monoalkylphosphoric acids that interfere with the lanthanide/actinide extraction.

From a more fundamental perspective, the ILs provide the unique opportunity to examine chemical processes commonly occurring in the degradation of nuclear waste and extraction solvents that have been very challenging to study, since such reactions typically occur in heterophase systems. The ability of the *ionic* liquids to integrate both ions and neutral molecules without phase separation allowed us to directly observe the interactions of the organic and inorganic components of the system for the first time.

Because the radiation chemistry of the NO_3^-/HNO_3, neat ILs, and dialkylphosphoric acids is very complex and many of the details remain poorly known, we preface the main discussion with a brief outline of the main features of this chemistry that are relevant for our study. Due to the large amount of data, some spectra and tables are placed in the Supporting Information and are designated with an "S" (such as Figure 1S). The complete list of abbreviations and notations used in this study and reactions 1−37 are also placed in the Supporting Information, for the reader's convenience.

2. RADIATION CHEMISTRY FUNDAMENTALS

2.1. Radiation Chemistry of Aqueous Solutions of NO_3^- and HNO_3. Despite many decades of research, even the aqueous radiation chemistry of nitrate systems is still insufficiently well-known, especially in concentrated solutions.[30−33] In dilute solutions, the dissociation constant for HNO_3 is 20 M^{-1},[31] so some HNO_3 molecules remain associated. In the following discussion, $e^{\bullet-}$ denotes the excess electron. Direct excitation of nitrate results in

the electron detachment (reaction 1a), N−O bond scission (reactions 1b−1e), or isomerization to peroxynitrite (reaction 1f):[30−33]

$$(NO_3^-)^{**} \rightarrow NO_3^{\bullet} + e^{\bullet -} \quad (1a)$$

$$(NO_3^-)^{**} \rightarrow NO_2^- + O(^3P) \quad (1b)$$

$$\rightarrow NO_2^{\bullet} + O^{\bullet -} \quad (1c)$$

$$\rightarrow NO^{\bullet} + O_2^{\bullet -} \quad (1d)$$

$$\rightarrow {}^3NO^- + {}^3O_2 \quad (1e)$$

$$\rightarrow ONOO^- \quad (1f)$$

with a reported branching ratio of 3:1 between reactions 1a and 1b (4.8 and 1.6 molecules decomposed for 100 eV radiation absorbed, respectively)[31] for low linear energy-transfer ionizing radiation. The analogous reactions for HNO_3 are

$$HNO_3^{**} \rightarrow NO_3^{\bullet} + e^{\bullet -} + H^+ \quad (2a)$$

$$HNO_3^{**} \rightarrow HNO_2 + O(^3P) \quad (2b)$$

$$\rightarrow NO_2^{\bullet} + HO^{\bullet} \quad (2c)$$

(with a reported yield of 4.8 and 2.2 molecules decomposed per 100 eV for reactions 2a and 2b), respectively).[31] Reactions 1b and 2b involve highly excited electronic states, and the direct experimental evidence for these reaction channels remains slim (see the discussion in refs 32 and 33). The recent studies[32] indicate that 6.2 eV photoexcitation of NO_3^- yields the cis-isomer of peroxynitrite, $ONOO^-$, via reaction 1f (with a quantum yield of 0.48) and reaction 1d or 1e (with a quantum yield of 0.08); reaction 1b was not observed. The resulting peroxynitrite easily protonates (the pK_a of ONOOH is 6.5−6.8) and slowly decomposes to $NO_2^{\bullet}$ and $HO^{\bullet}$ that can undergo recombination to regenerate HNO_3. The details of these (photo)reactions remain uncertain.[32,33]

Radiolysis of water produces $e^{\bullet -}$, $H^{\bullet}$, and $HO^{\bullet}$, whose major reactions in such nitrate-/nitrite-containing solutions are[30,31,34,35]

$$e^{-\bullet} + H_3O^+ \rightarrow H_2O + H^{\bullet} \quad (3)$$

$$HO^{\bullet} + HNO_3 \rightarrow H_2O + NO_3^{\bullet} \quad (4a)$$

$$HO^{\bullet} + NO_2^- \rightarrow HO^- + NO_2^{\bullet} \quad (4b)$$

$$e^{\bullet -} + NO_3^- \rightarrow NO_3^{\bullet 2-} \quad (5a)$$

$$e^{\bullet -} + NO_2^- + H_2O \rightarrow NO_2^{\bullet 2-} + H_2O \rightarrow NO^{\bullet} + 2HO^- \quad (5b)$$

$$H^{\bullet} + NO_3^- \rightarrow HO^- + NO_2^{\bullet} \quad (6a)$$

$$H^{\bullet} + NO_2^- \rightarrow HO^- + NO^{\bullet} \quad (6b)$$

The $NO_3^{\bullet 2-}$ radical has low stability in room-temperature aqueous solutions, rapidly ($\sim 10^3$ M^{-1} s^{-1})[36] hydrolyzing to yield $NO_2^{\bullet}$ (a similar reaction occurs not only in water but also in the presence of any (weak) acid, $H^{\delta +}B^{\delta -}$)

$$NO_3^{\bullet 2-} + H^{\delta +}B^{\delta -} \rightarrow B^- + HNO_3^{\bullet -} \quad (7a)$$

$$HNO_3^{\bullet -} \rightarrow HO^- + NO_2^{\bullet} \quad (7b)$$

This reaction is catalyzed by hydronium (4.5×10^{10} M^{-1} s^{-1}).[36] Similar, but faster reactions occur with many other organic and inorganic acids, including even such weak acids as alcohols, boric acid, and ammonia. Nitrous acid, in addition to ionization, can undergo reaction

$$2HNO_2 \rightarrow NO^{\bullet} + NO_2^{\bullet} + H_2O \quad (8)$$

$NO_x^{\bullet}$ (x = 1−3) can undergo cross-recombination to yield N_2O_m oxides (m = 3, 4, 5) that can either dissociate back to these radicals or hydrolyze to (protonated) NO_2^- (m = 3), $NO_2^- + NO_3^-$ (m = 4), and NO_3^- (m = 5).[31] These radicals also react with other radicals present in the irradiated solution. $NO_3^{\bullet}$ can also convert to $NO_2^{\bullet}$ via its reaction with radiolytically generated NO_2^- (4.4×10^9 M^{-1} s^{-1}) and HNO_2 (8×10^6 M^{-1} s^{-1}).[35] In aqueous solutions, $NO_3^{\bullet}$ is quite reactive toward various organic molecules[30,37] (as opposed to the same radical in the gas phase),[38,39] typically reacting by hydrogen abstraction (with aliphatic compounds)[38]

$$RH + NO_3^{\bullet} \rightarrow R^{\bullet} + HNO_3 \quad (9)$$

(the reaction rates are $(1-30) \times 10^6$ M^{-1} s^{-1}) or by addition to double bonds.[39] For substituted aromatic molecules the latter reactions can be quite rapid (10^7 to 3×10^9 M^{-1} s^{-1}), and these reactions result either in the oxidation of the molecule or H abstraction from a pending group in the vicinal position to the attached $NO_3^{\bullet}$.[37,39] Analogous reactions for $NO_2^{\bullet}$ are significantly slower or do not occur at all; still, the released $NO_2^{\bullet}$ can recombine with organic radicals ($R^{\bullet}$) present in the reaction mixture, yielding RNO and RNO_2 compounds.[40] Readily oxidizable organic radicals, such as ketyl radicals, can also be directly oxidized by $NO_2^{\bullet}$ to ketones:[40]

$$>C^{\bullet}OH + NO_2^{\bullet} \rightarrow >C{=}O + HNO_2 \quad (10)$$

The escape of the dimeric form of $NO_2^{\bullet}$ (N_2O_4) from the aqueous phase into the organic phase and subsequent cross-reactions with organic radicals generated in the diluent is the current conceptual picture of radiation damage in the nitric acid−organic diluent microemulsions that are formed during the extraction of decaying radionuclides.[9,40]

In irradiated frozen aqueous solutions of HNO_3 [41,42] and KNO_3,[41,43] the predominant species observed using electron paramagnetic resonance (EPR) spectroscopy are $NO_x^{\bullet}$ (x = 2, 3); in alkaline glasses, $NO_3^{\bullet 2-}$ is also observed. In crystalline alkali nitrates, all three of these radicals were observed,[43] and some researchers also postulated the formation of $NO^{\bullet}$, $NO_2^{\bullet 2-}$, and $ONOO^{\bullet}$, although the crowded EPR spectra make these identifications less reliable. The total yield of radicals[44] in the HNO_3/H_2O system rapidly increases with [HNO_3], reaching 16 per 100 eV in 12 M solution; in radiolysis of 1 and 5 M $NaNO_3$ at 77 K, the radical yield is 1 and 2.3 per 100 eV, respectively, with the radiolytic yield of the nitrite being 0.6 and 1.1 anions per 100 eV, respectively. $NO_3^{\bullet}$ and $NO_3^{\bullet 2-}$ both decay at around 150 K, while $NO_2^{\bullet}$ persists until the matrix softens around 200 K. The relative yield of $NO_3^{\bullet 2-}$ increases considerably in crystals (such as glycine nitrate)[45] as compared to aqueous solutions, suggesting that the stability of this radical (as well as that of $NO_2^{\bullet 2-}$) is controlled by the rate of protonation at low temperature.

2.2. Sketch of Radiation Chemistry of Neat Imidazolium ILs. In the following, the residue of the substituted imidazole with respect to the nth position in the aromatic ring (Scheme 1) is designated Q_n, so the parent cation is represented as Q_2H^+ or,

alternatively, as Q_1RH^+, the reduced cation as $Q_2H^\bullet$, and the H-atom adduct at carbon-2 as $Q_2H_2^{\bullet+}$, and the carbene as $Q_2^{\bullet\bullet}$, etc. Radiation-induced excitation of the constituent cations (Q_2H^+) and anions (A^-) leads to ionization of the constituent cations and electron detachment from the constituent anions from dissociative electronically excited states:[12−20]

$$(A^-)^{**} \rightarrow A^\bullet + e^{\bullet-} \quad (11)$$

$$(Q_1RH^+)^{**} \rightarrow Q_1RH^{\bullet 2+} + e^{\bullet-} \quad (12)$$

According to our EPR studies,[12,16] the radical dication deprotonates from the long aliphatic arm forming a C-centered alkyl radical $Q_1R^{\bullet+}$ (here B^- can be an extrinsic anion different from the constituent anion)

$$Q_1RH^{\bullet 2+} + B^- \rightarrow Q_1R^{\bullet+} + H^{\delta+}B^{\delta-} \quad (13)$$

Different types of such alkyl radicals are simultaneously present in the reaction mixture. The electron detachment and ionization may compete with other fragmentation reactions of excited ions, such as fragmentation of $(A^-)^{**}$ (of which reactions 1b−1f are examples)[12,15] and the elimination of the long arm from $(Q_1RH^+)^{**}$ (with the formation of the olefin and Q_1H^+) and C−C and C−H cleavage (from any position in the long arm) that compete with the ionization reaction 12.[16] It is likely that radical dications $Q_1RH^{\bullet 2+}$ generated in reaction 12 can undergo C−C cleavage and eliminate carbonium cations in addition to reaction 13 that subsequently deprotonate yielding olefins. In the following we will use $Q_1R^{\bullet+}$ as the symbol for *all* kinds of alkyl-type fragment radicals derived from the cation; spectroscopically; distinguishing between long-chain $R^\bullet$ and $Q_1R^{\bullet+}$ by means of EPR is often impossible.

The oxidized anions ($A^\bullet$) can also fragment. For example, oxidized $CH_3CO_2^-$ decarboxylates to $^\bullet CH_3$ and CO_2 while oxidized $CF_3SO_3^-$ dissociates to $^\bullet CF_3$ and SO_3.[15] Dissociative electron attachment to fluorinated anions results in fluoride loss; for $CF_3SO_3^-$, this reaction yields $^\bullet CF_2SO_3^-$; for NTf_2^-, it yields $^\bullet CF_2SO_2NTf^-$, and the excited $(NTf_2^-)^{**}$ can also fragment via

$$(NTf_2^-)^{**} \rightarrow CF_3SO_2^\bullet + TfN^{\bullet-} \quad (14)$$

$$TfN^{\bullet-} + Q_2H^+ \rightarrow Q_2(NHTf)^\bullet \quad (15)$$

$$CF_3SO_2^\bullet \rightarrow {}^\bullet CF_3 + SO_2 \quad (16)$$

The main electron-reduction pathway in the imidazolium ILs is[12,15,16]

$$e^{\bullet-} + Q_2H^+ \rightarrow Q_2H^\bullet \quad (17)$$

that competes with electron attachment to $H^{\delta+}B^{\delta-}$, when the latter acids are present in the IL solvent (such acids can be generated radiolytically via reaction 13 and other deprotonation reactions or be present in the ILs as an impurity):[15]

$$e^{\bullet-} + H^{\delta+}B^{\delta-} \rightarrow H^\bullet + B^- \quad (18)$$

These reactive $H^\bullet$ atoms either abstract hydrogen from the parent ions, e.g., the arms of the cations,

$$H^\bullet + Q_1RH^+ \rightarrow H_2 + Q_1R^\bullet \quad (19)$$

or add to the imidazolium ring[16]

$$H^\bullet + Q_2H^+ \rightarrow Q_2H_2^{\bullet+} \quad (20)$$

forming the adduct radical cation which is involved in a protic equilibrium with the reduced cation:

$$Q_2H^\bullet + H^{\delta+}B^{\delta-} \rightleftharpoons Q_2H_2^{\bullet+} + B^- \quad (21)$$

For imidazolium cations that are not alkyl substituted at carbon-2, this equilibrium is shifted to the right side.[16] $Q_2H^\bullet$ is also involved in another equilibrium reaction, with its own parent cation,

$$Q_2H^\bullet + Q_2H^+ \rightleftharpoons (Q_2H)_2^{\bullet+} \quad (22)$$

that yields a C(2)−C(2) $\sigma^2\sigma^{*1}$ bound dimer radical cation.[13−16] In most of the ILs equilibrium reaction 22 is shifted to the left side, but, in some ILs (that are composed of bulky anions, such as NTf_2^-), it is shifted to the right side.[13,16] As seen from this brief account, the resulting reaction mixture contains many types of organic and inorganic radicals. These radicals (cross-)recombine and undergo secondary chemistry (such as the addition of these radicals to the parent cation); the resulting chemistry is complex.

As the ILs preequilibrated with aqueous solutions contain a fair amount of water (15−20 mol %), another useful reference system is an aqueous solution of a water-soluble IL. The most relevant known reactions for this study are the oxidation of the imidazolium cation by hydroxyl radicals and other oxidizing radicals.[46] Retrospectively, the original reaction scheme (that involved the addition to carbon-4,5) suggested in ref 46 needs be revised to

$$HO^\bullet + Q_2H^+ \rightarrow Q_2H(OH)^{\bullet+} \quad (23a)$$

$$Q_2H(OH)^{\bullet+} \rightleftharpoons Q_2(OH)^\bullet + H^+ \quad (23b)$$

Behar et al.[46] postulated that $SO_4^{\bullet-}$ (a strong oxidizer) can directly cause one-electron oxidation of the imidazolium cation with the formation of relatively stable hydrated $Q_1RH^{\bullet 2+}$

$$SO_4^{\bullet-} + Q_1RH^+ \rightarrow Q_1RH^{\bullet 2+} + SO_4^{2-} \quad (24)$$

The absorption spectrum of this dication radical was surprisingly similar to that of the $Q_2H_2^{\bullet+}$ and $Q_2H(OH)^{\bullet+}$ radical adducts. This observation contradicts our EPR results that indicate quantitative deprotonation of $Q_1RH^{\bullet 2+}$ even at low temperature[7,12,15,16] (as well as the later observations of Behar et al.[47] on pyridinium ILs), and in section 5 we suggest a reinterpretation of these observations. The relevance of reaction 24 for this work is that the analogous reaction can be expected for another oxidizing radical, $NO_3^\bullet$ (as both $SO_4^{\bullet-}$ and $NO_3^\bullet$ first add to the aromatic rings before the oxidation, and the $NO_3^\bullet$ is known to react rapidly with many alkyl-substituted aromatic molecules; see section 2.1).

In ref 15 we presented preliminary results on the radiolysis of nitrate anions in frozen ILs. In C_2mim BF_4:NO_3 (1:1 (w/w)) glass irradiated at 77 K, the EPR spectrum was mainly from $NO_2^\bullet$ and $NO_3^{2-\bullet}$; no $NO_3^\bullet$ were observed in this IL and tetrabutylammonium nitrate ($N_{4444}NO_3$). The formation of these two radicals suggested that reactions analogous to reactions 5a, 6a, and 7 were occurring in the ILs. Warming of the irradiated $N_{4444}NO_3$ caused the decay of these radicals and the formation of a radical whose spin parameters were similar to those of $NO_2^{\bullet 2-}$ in alkali nitrite crystals, suggesting thermally activated charge-transfer reaction

$$NO_3^{\bullet 2-} + NO_2^- \rightarrow NO_3^- + NO_2^{\bullet 2-} \quad (25)$$

involving radiolytically generated nitrite anions.

2.3. Dialkylphosphoric Acids. The two main products observed in irradiated $HO(O)P(OR)_2$ are ROH, $(HO)_2(O)POR$, phosphoric acid (suggesting secondary dealkylation reactions), H_2, and hydrocarbons.[9] The mechanism for radiolysis of $HO_2P(OR)_2$ and $^-O_2P(OR)_2$ is less understood than that of trialkylphosphates, $OP(OR)_3$,[48,49] but the main reactions are similar,[50−54] involving (i) homolytic P−O cleavage in the excited state of the parent molecule leading to the formation of P-centered phosphoryl and alkoxy radicals, (ii) one-electron reduction followed by fragmentation, and (iii) oxidation of aliphatic groups (mainly, at the α-position), possibly coupled to the protonation of the $>PO_2^-$ moiety (similar to reactions 12 and 13). Elimination of the olefin radical $^\bullet R(-H_2)$ (reaction 28b)[53,54] has been suggested as an alternative to the latter reaction in order to explain the occurrence of dealkylation in the presence of electron scavengers, but there is no direct evidence for this reaction. As the chemistry of the alkali dialkylphosphates is better understood, we give the corresponding reactions for the anionic form; it is easy to rewrite these equations for the protonated form:

$$^-O_2P(OR)_2{}^{**} \rightarrow RO^\bullet + ROP^\bullet O_2{}^{2-} \quad (26)$$

$$^-O_2P(OR)_2 + e^{\bullet -} \rightarrow (RO)_2P^\bullet O_2{}^{2-} \quad (27a)$$

$$^-O_2P(OR)_2 + e^{\bullet -} \rightarrow RO^- + ROP^\bullet O_2{}^- \quad (27b)$$

$$^-O_2P(OR)_2 + e^{\bullet -} \rightarrow R^\bullet + ROPO_3{}^{2-} \quad (27c)$$

$$^-O_2P(OR)_2 + h^{\bullet +} \rightarrow \{^\bullet R(-H)O\}(RO)PO_2H \quad (28a)$$

$$^-O_2P(OR)_2 + h^{\bullet +} \rightarrow ROPO_3H_2 + {}^\bullet R(-H_2) \quad (28b)$$

In the EPR spectra of irradiated frozen $(MeO)_2PO_2Na$, in addition to the methyl, phosphoryl ($MeOP^\bullet O_2^-$), and $^\bullet CH_2OP\sim$ radicals,[50,51] the formyl ($HC^\bullet O$)[50] and phosphoranyl ($(MeO)_2P^\bullet O_2{}^{2-}$) radicals have been observed.[48−51,53] Only *phosphoryl* radicals are observed in irradiated methanol solutions of $(MeO)_2PO_2Na$ and room-temperature alkali salts, suggesting poor stability of the intermediate phosphoranyl radicals. In ref 15 we examined $C_n$mim $(MeO)_2PO_2$ and found no evidence for P-centered and methyl radicals in such ILs. Instead, we observed $^\bullet CH_2OH$ and, possibly, $^\bullet CH_2OP\sim$. Above 150 K, these two radicals added to carbon-2 in the imidazolium ring forming the corresponding radical C(2)-adducts. Because none of the previously suggested reactions account for the formation of the hydroxymethyl radical (which is formed by the internal rearrangement of the methoxy radical), we suggested that the oxidized anion undergoes dephosphorylation:

$$^-O_2P(OR)_2 + h^{\bullet +} \rightarrow RO^\bullet + ROPO_2 \quad (28c)$$

Furthermore, the formation of the formyl radical in dimethylphosphate radiolysis[50] suggests that the excited-state C-centered radical generated in reaction 28a might eliminate formaldehyde (reaction 29a) with the phosphoryl radical abstracting hydrogen from the leaving CH_2O, forming the phosphinate (reaction 29b):

$$^\bullet CH_2O(MeO)PO_2H{}^{**} \rightarrow CH_2O + MeO^\bullet PO_2H \quad (29a)$$

$$CH_2O + MeO^\bullet PO_2H \rightarrow HC^\bullet O + MeO(H)PO_2H \quad (29b)$$

Alternatively, the formaldehyde is generated via disproportionation of hydroxymethyl radicals generated in reaction 28c and the formyl radical is generated via the secondary reactions of the formaldehyde with primary radicals. In addition to the electron-scavenging reactions given above, the protonated form of the dialkylphosphates, as with all acids, can undergo dissociative electron attachment reaction 18 with the release of H atoms that abstract hydrogen from the aliphatic tails of the solvent ions and the solute and add to the imidazolium ring. As we argue below, in the imidazolium ILs, the main reductive pathway for the dialkylphosphoric acids is reaction 18 rather than reactions 27.

3. EXPERIMENTAL AND COMPUTATIONAL METHODS

The reagents used in this study have been obtained from Aldrich except for C_{10}mim NTf_2 that was synthesized in M. L. Dietz's laboratory at the University of Wisconsin, Milwaukee using a previously reported synthetic approach.[2] Synthetic, spectroscopic, and computational approaches used in this study were similar to those used in prior work.[7,12−16] The samples were frozen by immersion in liquid nitrogen and irradiated to 3 kGy (1 Gy = 1 J/kg) at 77 K using 3 MeV electrons. The radicals were observed using a 9.44 GHz Bruker ESP300E spectrometer, with the sample placed in a flow He cryostat (Oxford Instruments CF935). The magnetic field and the hyperfine coupling constants (hfcc) are given in the units of gauss (1 G = 10^{-4} T). If not stated otherwise, the first-derivative EPR spectra were obtained at 50 K using 2 G modulation at 100 kHz. Second-derivative EPR spectra were obtained by the numerical differentiation. The radiation-induced EPR signal from the E'_γ center in the Suprasil sample tubes was deleted from the EPR spectra. To conserve space, some figures have been placed in the Supporting Information. Such figures have designator "S" (e.g., Figure 1S).

We used the $C_n$mim NO_3 as supplied; as suggested by ^{1}H NMR measurements, these samples contained 10 mol % water; the fraction of water in dried samples of other imidazolium liquids was 1−2 mol % except for $C_n$mim AcO that contained 19 mol % of "protons" (probably, in the form of H_3O^+) with a chemical shift of 11.13 ppm in dimethyl-d_6 sulfoxide. These NMR spectra were obtained using a 500 MHz Bruker Avance 3 spectrometer. Some experiments were carried out with imidazolium ILs in which H(2,4,5) protons were exchanged for deuterium; the exchange protocols followed the method reported previously.[7,15,16] The experiments on nitric acid doped ILs proceeded as follows: C_{10}mim NTf_2 was vortexed for 5 min with a solution of 3 M DNO_3 in D_2O (1:1 (v/v)); the solution was then equilibrated for 1 h and subsequently separated by centrifuging at 6000 rpm for 15 min. The concentration of the nitrate in the IL phase was determined using ^{14}N NMR with CH_3NO_2 as the internal standard. The IL solution formed a clear, glassy solid upon rapid freezing at 77 K. Alternatively, we introduced 10 mol % D_2O into water-miscible C_4mim TfO, with a variable amount of concentrated DNO_3 added to it.

The calculations of the hfcc and the structures for the radicals were carried out using a density functional theory (DFT) method with the B3LYP functional[55] and 6-31+G(d,p) basis set from Gaussian 98.[56] In the following, a denotes the isotropic hfcc and B denotes the principal values of **B**, that is the anisotropic part of the hfc tensor **A**. Simulations of the EPR spectra involved angular averaging of the fixed-tensor radicals using first-order perturbation theory; for phosphoranyl and phosphoryl radicals, second-order corrections were used.

Product analyses were performed using ^{1}H NMR (with $CDCl_3$ used as a solvent and tetramethylsilane, TMS, used as

Table 1. Principal Values of g-Tensors and Hyperfine Tensors for ^{14}N in Nitrate-Derived Radicals

attribution	δg_x [a]	δg_y	δg_z	A_{iso}, G	B_{xx}, G	B_{yy}, G	B_{zz}, G	system
$NO_2^{\bullet}$	65 (66) [b]	31 (22)	−79 (−80)	54 (56.9)	−5.8 (−6.3)	12.6 (13.3)	−6.8 (−7.2)	C_4mim TfO + 0.5 M DNO_3
$NO_2^{\bullet}$	61	24	−78	55	−5.8	12.6	−6.8	C_{10}mim NTf_2 1:1 v/v 3 M DNO_3
$NO_3^{\bullet 2-}$	37 [c]	71	71	40.7	17.3	−8.7	−8.7	N_{4444} NO_3 50 K
	31 (21)	78 (65)	60 (60)	40.8 (52.2)	18.9 (20.8)	−9.3 (−11.2)	−9.7 (−9.7)	
$NO_2^{\bullet 2-}$	37 (29)	79 (78)	79 (78)	25.6 (15.3)	17.9 (21.9)	−9.0 (−11)	−9.0 (−11)	N_{4444} NO_3 225 K
$Q_2N(O^{\bullet})OH$	100	71	33	8.5	−8.5	−8.5	25.3	C_4mim AcO:NO_3 (1:1), 200 K
$NO_3^{\bullet}$	(230)	(230)	(31)	3.7	−0.3	−0.3	0.6	KNO_3

[a] $\delta g = (g - 2) \times 10^4$; the **g**- and **A**-tensors were assumed to be coaxial. Literature parameters are given in the parentheses. [b] In ice. [c] Assuming axial tensors.

the chemical shift standard)[8] and tandem electrospray mass spectrometry in the positive (MS_1^+) or negative (MS_1^-) modes using a spray voltage of 4.5 kV; acetonitrile was used as the solvent.[16] The sealed samples prepared for these analyses were placed in a thin-wall diameter 10 mm NMR tube and irradiated using the same 3 MeV electron accelerator facility at the dose rate of 680 Gy/s to the cumulative dose of 1−2.5 MGy; the sample was cooled by flowing chilled water so that the internal temperature during the electron irradiation was less than 40 °C.

4. RESULTS

4.1. Electron Scavenging by Protic Solutes. Because both the dialkylphosphoric and nitric acids are special examples of *acids*, it is prudent first to examine the generic reaction of protic solutes in ILs before these particular instances are considered in more detail.

Our previous research (section 2.2) suggested that the protic impurity ($H^{\delta+}B^{\delta-}$, reaction 18) can compete with the parent imidazolium cations (reaction 17) as the acceptor of the electrons generated through reactions 1a, 11, and 12, resulting in the formation of $H^{\bullet}$ atoms; at higher temperature (170−220 K), the acid can also protonate 2-imidazolyl radicals (reaction 21). To study these reactions, we used hydrogen sulfate (HSO_4^-) as the progenitor of the $H^{\bullet}$ atoms. In neat C_2mim HSO_4 at 77 K, the H atoms released in reaction 18 promptly added to the parent cation via reaction 20.[15] This low-temperature reaction allows quantifying of the relative yield of reaction 20, as the resulting $Q_2H_2^{\bullet+}$ radical cation has two equivalent protons with large hfcc's (∼40 G) (Table 1S and Figures 1S and 2S in Supporting Information) and the corresponding resonance lines (indicated with open circles in Figure 2S) of the H-atom adduct are spectrally separated from the resonance lines of the $Q_2H^{\bullet}$ radicals. These lines, however, overlap with the resonance lines of $Q_1R^{\bullet+}$. $Q_2H^{\bullet}$ and $Q_1R^{\bullet+}$ decay when the sample is warmed to 200 K, and the triplet of the $Q_2H_2^{\bullet+}$ radicals can be observed without interference from other radical species; the EPR spectrum (shown in Figure 2S) exhibits the characteristic multiplet with a 7 G separation of the resonance lines resulting from the hfcc's on the $^1H_\alpha$ and $^{14}N_{1,3}$ nuclei (Table 1S and Figure 1S). The characteristic doublet of $Q_2H^{\bullet}$ spectrally overlaps with the $M_z(2^1H_2) = 0$ component of the $Q_2H_2^{\bullet+}$ radical, so only the $M_z(2^1H_2) = \pm 1$ side lines can be used for quantitative characterization. To this end, the first-derivative EPR spectra obtained for C_2mim BF_4:HSO_4 mixtures were normalized by the double integral of the spectrum (which is proportional to the radical yield) and the intensity of the $M_z(2^1H_2) = +1$ line of $Q_2H_2^{\bullet+}$ superimposed on the broad line of $Q_1R^{\bullet+}$ was estimated as the difference in the EPR signals at the center of the corresponding band, as shown in Figure 3S(a). As shown in ref 15, neither BF_4^- nor HSO_4^- anions yield interfering EPR signals; all of the resonance lines observed in these IL systems are from the cation-derived radicals. It is seen from Figure 3S(a,b) that the relative yield of $Q_2H_2^{\bullet+}$ systematically increases relative to the yield of $Q_2H^{\bullet}$ as the mole fraction of C_2mim HSO_4 increases, reflecting the competition between reactions 17 and 18. When the concentration of $[HSO_4^-] \approx 1$ M (15.3 mol %), 50% of the maximum effect is reached.

These observations indicate that C_2mim^+ (that are present at 6.5 M in C_2mim BF_4) can compete with the protic electron scavengers, such as HSO_4^-, unless there is high concentration of the latter. This behavior distinguishes the aromatic ILs from aliphatic ILs (that involve, e.g., quaternary ammonium, phosphonium, and pyrrolidinium cations) in which there is no such competitive electron scavenging.

4.2. Nitrate and Nitric Acid. *4.2.1. Electron Scavenging.* In ref 15, we examined EPR spectra of crystalline tetrabutylammonium nitrate ($N_{4444}NO_3$) and glassy $C_n$mim BF_4:NO_3. For $N_{4444}NO_3$, the EPR spectrum observed at 50−120 K was mainly from $NO_3^{\bullet 2-}$ (Figure 4S, lower trace) with some weaker features that we attributed to $NO_2^{\bullet}$; above 220 K, both of these radicals disappeared and another radical emerged (Figure 4S, upper trace) whose **g**- and **A**-tensors most closely matched the reported parameters for $NO_2^{\bullet 2-}$ (see Table 1). In Figure 5S, we simulated the spectra of $NO_3^{\bullet}$ and $NO^{\bullet}$ radicals using the parameters reported in the literature; it is observed that these radicals are not generated either in this system or (as shown below) in other ILs. In hindsight, our analysis of the 50 K spectrum[50] was incorrect due to the EPR signal overlap that was not adequately taken into account. In Figure 6S(b), we simulated the composite spectrum as the weighed sum of the signals from $NO_2^{\bullet}$ (trace i, with the parameters determined, subsequently explained as follows, Figure 6S(a) and Table 1) and $NO_3^{\bullet 2-}$ (trace ii); the best agreement was achieved assuming 1:7.7 ratio between the radical concentrations, respectively. In this simulation, the parameters of $NO_2^{\bullet}$ were fixed (using the analysis described below), while the parameters for $NO_3^{\bullet 2-}$ were optimized. In Figure 1, we demonstrate that the same two radical species (no change in magnetic parameters) can also account for the EPR spectra (77 K) observed in irradiated C_2mim BF_4:NO_3 (1:1.15 (mol/mol)) and C_4mim PF_6:NO_3 (1:1 (mol/mol)), but the ratio changes to 2.45:1 and 1:1, respectively; the residual differences between the simulated and observed EPR spectra are due to the interference from radicals derived from the parent cations. Thus, in tetrabutylammonium nitrate, which contains no proton donors for reactions 7 to occur, the yield of $NO_2^{\bullet}$ is low and the main source of N-centered radicals is electron scavenging by nitrate that yields

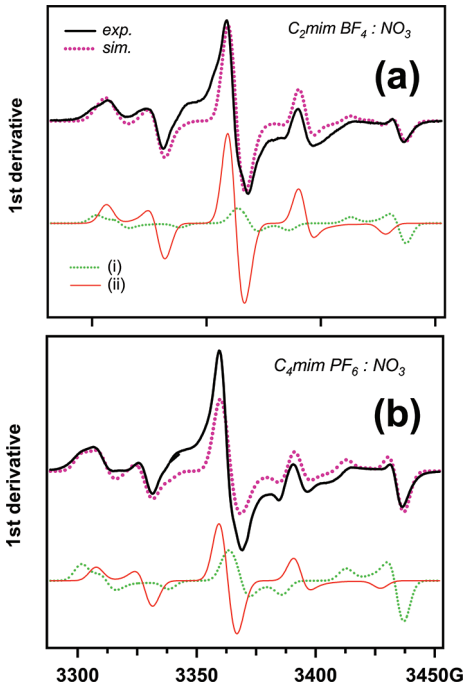

Figure 1. Comparison of experimental (bold solid lines) and simulated (bold dotted lines) first-derivative EPR spectra for (a) irradiated C_2mim BF_4:NO_3 (1:1.14 (mol/mol)) and (b) C_4mim PF_6:NO_3 (1:1 (mol/mol)) obtained at 50 K after 3 MeV electron beam radiolysis at 77 K. The dotted lines are weighed sums of the two contributions, from (i) $NO_2^\bullet$ and (ii) $NO_3^{\bullet 2-}$; these decompositions are shown at the bottom of both panels. The simulation parameters are given in Table 1. The X-band EPR spectra were obtained for a microwave power of 2 mW and modulation amplitude of 2 G (100 kHz modulation).

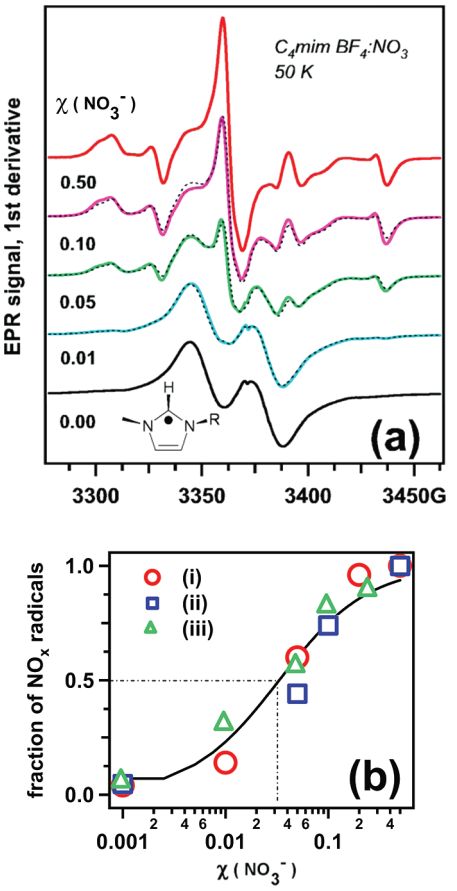

Figure 2. (a) EPR spectra from irradiated C_4mim BF_4:NO_3 samples (solid lines). The mole fraction χ of the nitrate is indicated in the plot. The dashed lines are weighed sums of the $\chi = 0$ and $\chi = 0.5$ spectra. These spectra were normalized by their double integral (that is, the total radical yield). (b) Relative fraction of the nitrate-derived radicals in the total radical yield for $C_n$mim A:NO_3 glasses irradiated at 77 K (as determined from the EPR spectra observed at 50 K), for (i) $n = 4$, A = PF_6; (ii) $n = 4$, A = BF_4, and (iii) $n = 10$, A = NTf_2. See also Figures 8S and 9S in the Supporting Information. The dashed−dotted lines indicate the mole fraction of the nitrate corresponding to 50% electron scavenging capacity (C_{50}).

$NO_3^{\bullet 2-}$. This situation is reversed in nitrate-doped imidazolium ILs, where the $NO_3^{\bullet 2-}$ is partially converted to $NO_2^\bullet$ via reactions 7 that may involve traces of water and acids or the parent imidazolium cations that are weakly acidic (producing the stable N-heterocyclic carbene, $Q_2^{\bullet\bullet}$)

$$Q_2H^+ \rightleftharpoons Q_2^{\bullet\bullet} + H^+ \qquad (30)$$

If the protonation of $NO_3^{\bullet 2-}$ (which is a strong base) indeed involves the deprotonation of the parent cation via reaction 30, the 2-yilidene $Q_2^{\bullet\bullet}$ would react with the resulting $NO_2^\bullet$, so the overall reaction is likely to be concerted; so it should be written as

$$NO_3^{\bullet 2-} + Q_2H^+ \rightarrow HO^- + Q_2(NO_2)^\bullet \qquad (31)$$

When the IL is doped with HNO_3 rather than NO_3^-, the reduction of HNO_3 should yield $NO_2^\bullet$ by dissociative electron attachment to HNO_3. Due to reactions 7, given the acidity of the HNO_3-doped solutions, every such electron-trapping event should result in formation of a $NO_2^\bullet$ radical. Furthermore, even if some of the electrons are scavenged by the protons (reaction 18) yielding $H^\bullet$ atoms, the latter species can be expected to react with the nitrate (or nitric acid) via reaction 6a rather than the parent cations via reactions 19 and 20, further increasing the yield of $NO_2^\bullet$.

In Figure 7S, we compare the EPR spectra observed in 6 M DNO_3 in D_2O with the EPR spectra obtained from irradiated (i) C_{10}mim NTf_2 preequilibrated with 3 M DNO_3 in D_2O and (ii) C_4mim TfO containing 10 vol % D_2O and 0.5 M DNO_3. The ^{14}N NMR measurements indicate that the concentration of the HNO_3/NO_3^- in solution I is ~0.16 M (6.3 mol %). The EPR spectra observed in these two IL systems (two upper traces in Figure 7S) are almost identical, and the comparison with the aqueous nitric acid (lower traces in Figure 7S) suggests that the main radical species observed in all three spectra is $NO_2^\bullet$. In the frozen aqueous solution, the EPR signal from $NO_3^\bullet$ (which is most visible in the 150 K trace, because $NO_2^\bullet$ fully decays at this temperature) superimposes onto the resonance lines of $NO_2^\bullet$; this $NO_3^\bullet$ signal is not observed in the IL solutions. The comparison of the computer simulations of the EPR spectrum of $NO_2^\bullet$ (see Table 1 for the simulation parameters) and the spectrum observed in the IL solutions suggests that $NO_2^\bullet$ *is the prevalent radical species generated in the radiolysis of such solutions.*

In Figure 2a, a scavenging experiment similar to that for HSO_4^- (section 4.1) was carried out with C_4mim BF_4:NO_3; Figures 8S and 9S in the Supporting Information present the results for the related C_4mim PF_6:NO_3 and C_4mim NTf_2:NO_3 systems, respectively. As shown in these three plots, first-derivative EPR

dx.doi.org/10.1021/jp206579j |J. Phys. Chem. B 2011, 115, 10927–10942

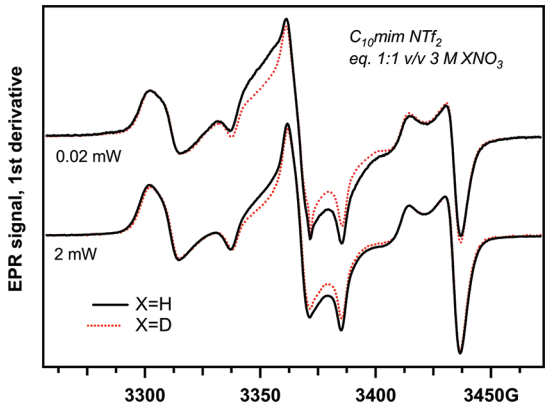

Figure 3. EPR spectra of frozen C_{10}mim NTf_2 preequilibrated with 1:1 (v/v) 3 M XNO_3 in X_2O, where X = H (solid lines) or X = D (dashed lines), and irradiated at 77 K. These spectra were obtained at two microwave power levels and different isotope compositions to illustrate that most of the EPR signal is from a single radical species, nitrogen dioxide. The same EPR spectrum is observed in C_4mim $TfO:D_2O$ containing 0.5 M DNO_3 (trace ii in Figure 7S) and frozen 6 M DNO_3 in D_2O.

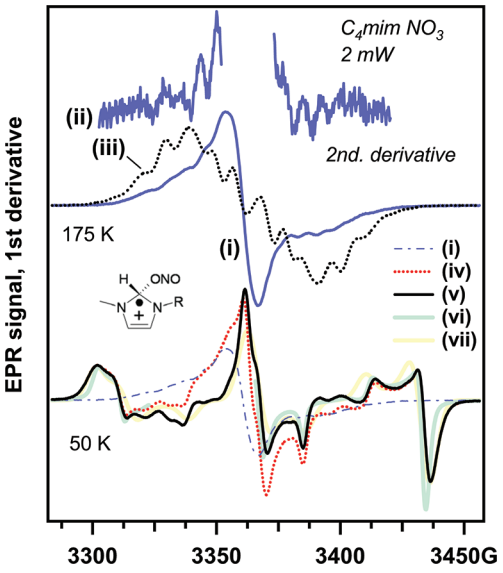

Figure 4. First derivative EPR spectra from irradiated C_4mim NO_3. Trace i is obtained after warming the sample irradiated at 77 K to 175 K and trace ii is the second derivative spectrum exhibiting a 7 G pattern from $Q_2HX^{\bullet+}$. Comparison with the EPR spectra of such adduct radicals simulated in Figure 1S suggests that the substituting group X is either -ONO or -OH (trace iii). The EPR spectrum obtained at 50 K (trace iv) can be decomposed into the contribution from the radical species also contributing to trace (i) and another signal (trace (v)) that strongly resembles the EPR spectrum of $NO_2^{\bullet}$ as observed in irradiated 6 M DNO_3 in D_2O (trace vi) or our simulation for this radical using the parameters given in Table 1 (trace vii).

spectra (normalized by their double integrals) at intermediate nitrate concentrations can be represented by the weighed sums of the spectra from neat C_4mim A (A = BF_4^-, PF_6^-, NTf_2^-) and the mixture of these ILs containing 25−50 mol % nitrate (dashed lines). Plotting this weight vs the mole fraction of the nitrate gives the concentration plots shown in Figure 2b. As seen from this plot, 50% electron scavenging is achieved at 3 mol % of the nitrate, which corresponds to 0.07 M NO_3^- for C_{10}mim NTf_2. It is seen, therefore, that the nitrate is a more efficient electron scavenger than HSO_4^-; the undissociated nitric acid should be still a stronger electron scavenger.

It is apparent from these EPR spectra and the thermal evolution of the EPR spectra for C_2mim BF_4:NO_3 shown in Figure 10S that $Q_2H^{\bullet}$ radical (which is observed at low nitrate concentration) is either strongly reduced or completely absent in the 50 mol % nitrate solutions. Closer examination of the EPR spectra obtained for C_4mim NTf_2:NO_3 solution (Figure 11S) indicated that introduction of nitrate resulted in a 3× decrease in the relative yield of $CF_3^{\bullet}$ and $^{\bullet}CF_2SO_2Tf^-$ generated via the dissociation of the excited $(NTf_2^-)^{**}$ anion (reactions 14−16), suggesting that the nitrate serves as a quencher of these dissociative excited states or prevents their formation from the recombination of electrons with $NTf_2^{\bullet}$.

What happens when the ILs are doped with nitric acid instead of nitrate? In the absence of DNO_3, the EPR spectrum from irradiated D_2O-saturated C_{10}mim NTf_2 (Figure 12S) was virtually identical to that of dry neat IL, in which the strong doublet of $(Q_2H)_2^{\bullet+}$ is superimposed on the broad spectrum from the $Q_1R^{\bullet+}$ radicals. In the presence of >0.1 M DNO_3, the EPR signal from $(Q_2H)_2^{\bullet+}$ entirely disappears, while the EPR signal from $Q_1R^{\bullet+}$ either disappears or becomes unobservable due to the strong overlap with the lines of $NO_2^{\bullet}$ (Figure 3) that disappear above 125 K (Figure 13S). The implication of these observations is that even trace amounts of nitric acid are sufficient to divert the reductive path toward the reduction of the solute.

4.2.2. Fragmentation of the Nitrate Anion. $NO_2^{\bullet}$ also makes the largest contribution to the EPR spectrum observed from irradiated wet (10 mol % water by ^{1}H NMR) C_4mim NO_3 (Figures 4 and 14S). As the temperature increases over 150 K (Figure 14S), $NO_2^{\bullet}$ decays and the residual spectrum persists to 200 K (trace I in Figure 4). By changing microwave power, it can be shown that this residual EPR spectrum is composite, consisting of a narrow singlet and a broad doublet (as the two radical species saturate at different power, having different spin relaxation times). The second-derivative spectrum for the 175 K trace (trace ii in Figure 2) reveals a 7 G modulation pattern which is typical for the adduct $Q_2YX^{\bullet+}$. The striking feature of this spectrum is that the spacing between the two major components of the doublet is significantly reduced as compared to $Q_2HX^{\bullet+}$ we previously observed (Table 1S and Figure 1S).

In section 5 we demonstrate that the proton coupling for H(2) in $Q_2HX^{\bullet+}$ is reduced in the presence of electron-withdrawing groups (such as X = OR), suggesting that the substituting group X at carbon-2 is -OH, -ONO, or -ONO_3 but not -NO_2 (Figure 1S and trace iii in Figure 4). Conversely the narrow signal can be accounted for by the $Q_2(OH)^{\bullet}$ or $Q_2(NO_2)^{\bullet}$ radicals, both of which have negligible hfcc for nuclei in C(2) substituting groups (Table 2S and Figure 1S). A closer examination of the EPR spectrum obtained at 50 K (trace iv in Figure 4) suggests that the same two radicals are already present at this temperature, but their weaker signals overlap with the stronger signal of $NO_2^{\bullet}$. When the EPR signal is subtracted (taking the scaled 175 K spectrum as the signal from these radicals), the residual trace v in Figure 4 closely matches the spectrum of $NO_2^{\bullet}$ obtained in irradiated 6 M DNO_3 (trace vi therein) and the simulated spectrum of this radical (trace vii therein).

While the narrow-line signal can be accounted for either by $Q_2(OH)^{\bullet}$ or $Q_2(NO_2)^{\bullet}$ (the latter presumably generated via reaction 31), the C(2) adduct radical (that is, protonated

2-imidazolyl) can be $Q_2H(OH)^{\bullet+}$, but it cannot be $Q_2H(NO_2)^{\bullet+}$ (section 5). The most likely channel for the formation of such (formally) "adduct" radicals is protonation of 2-imidazolyl radicals rather than the reactions of $HO^\bullet$ (reaction 23a) and $NO_2^\bullet$ with the cation. Indeed, the hydroxyl radical should have fully reacted at 50 K, whereas $NO_2^\bullet$ have negligible reactivity below 200 K. Thus, the most likely explanation for these results is by assuming the prompt formation of $Q_2(OH)^\bullet$ and $Q_2H(OH)^{\bullet+}$ in low-temperature radiolysis with a consequent increase in the $Q_2H(OH)^{\bullet+}$ yield due to forward reaction 23b. This can be explained provided that, in radiolysis of $C_n$mim NO_3, the direct excitation of the nitrate mainly results in reaction 1c and the release of $NO_2^\bullet$ and $O^{\bullet-}$. We suggest that the latter reacts with the parent cation:

$$O^{\bullet-} + Q_2H^+ \rightarrow Q_2(OH)^\bullet \quad (32)$$

yielding the 2-hydroxyimidazolyl radical. Alternatively, $O^{\bullet-}$ is protonated to $HO^\bullet$, and the resulting hydroxyl radical adds to the imidazolyl ring (reaction 23a); the two resulting radicals can be transformed into each other by reactions 23b.

4.2.3. Oxidation Pathway. $NO_3^\bullet$, which is one of the main oxidation products of aqueous HNO_3/NO_3^- solutions, is absent from the EPR spectra of the irradiated IL solutions. Either reaction 1a does not occur in the ILs, that is the corresponding excited-state transfers energy to an organic cation faster than it autoionizes, or $NO_3^\bullet$, which is a strong oxidizer, is inherently unstable in these ILs. In what follows, we examine the experiment aiming to observe the possible interference with the oxidative pathway. To this end, we added nitrate to C_2mim CH_3CO_2, which has a readily oxidizable acetate anion that yields methyl and carboxymethyl radicals, whose sharp resonance lines can be distinguished against the background signals from other radicals present in the reaction mixture:

$$(CH_3CO_2^-)^{**} \rightarrow {}^\bullet CH_3 + CO_2 + e^{\bullet-} \quad (33a)$$

$$(CH_3CO_2^-)^{**} \rightarrow {}^\bullet CH_2CO_2^- + H^+ + e^{\bullet-} \quad (33b)$$

As shown in Figure 15S, addition of the nitrate has only minor effect on the relative yield of ${}^\bullet CH_3$ and ${}^\bullet CH_2CO_2^-$ (to the total radical yield). Furthermore, as is the case for other $C_n$mim A:NO_3 systems (section 4.2.1), the EPR spectra observed at intermediate nitrate concentrations can be simulated by weighing the spectra observed in IL solvent containing 0 and 50 mol % nitrate (Figures 15S for $n = 2$ and Figure 16S for $n = 4$, respectively). The relative yield of the $NO_2^\bullet$, as judged from the growth of the $M_z(^{14}N) = +1$ line or weighing of the spectra in Figures 15S and 16S is approximately linear with the mole fraction of nitrate (Figure 17S). When the irradiated C_2mim CH_3CO_2 is warmed to 200 K, the EPR spectra undergo several transformations (Figure 18S). At 130 K, the methyl radicals disappear and the residual EPR signal is mainly from the carboxymethyl radical. At 170 K, this carboxymethyl radical decays and the residual EPR signal is from the $Q_2HX^{\bullet+}$ adduct, where X could be either the methyl or carboxymethyl groups (this is seen from the second-derivative spectra shown in Figure 19S). These transformations are accounted for by thermally activated H-abstraction and ring addition by small, mobile radicals:

$${}^\bullet CH_3 + CH_3CO_2^- \rightarrow CH_4 + {}^\bullet CH_2CO_2^- \quad (34a)$$

$$X^\bullet + Q_2H^+ \rightarrow Q_2HX^{\bullet+} \quad (X = CH_3,\ CH_2CO_2^-) \quad (34b)$$

Similar transformations were also observed for C_4mim CH_3CO_2 (Figure 20S). In both cases (Figures 21S and 22S), the outermost lines from $Q_1R^\bullet$ can be observed even in the presence of $NO_2^\bullet$, and the comparison between the normalized EPR spectra indicates that the relative yield of the $Q_1R^\bullet$ radicals *increases* in the presence of nitrate (by ~20% in C_4mim CH_3CO_2 containing 50 mol % nitrate).

Above 200 K, all radicals in neat C_4mim CH_3CO_2 except for $Q_2HX^{\bullet+}$ decay, but in the presence of nitrate, another radical is observed (Figure 20S), which is similar in appearance in C_2mim BF_4, C_2mim CH_3CO_2, and C_4mim CH_3CO_2. This spectrum can be simulated using the set of parameters given in Table 1 (see the simulations in Figure 23S). This set does not correspond to any known NO_x radical; among the known N-centered organic radicals, it is most consistent with aryl-substituted nitroxide with $a(^{14}N) \approx 8.5$ G and $B_\parallel(^{14}N) \approx 16.8$ G. This identification would also explain the persistence of this radical at high temperature. Our DFT calculations for the planar $Q_2{}^+N(O^\bullet)OH$ give negligible (<3 G) hfcc in the OH and the ^{14}N and ^1H nuclei in the imidazolium ring and $a(^{14}N) \approx 7.9$ G and $B_\parallel(^{14}N) \approx 13.3$ G. We, therefore, suggest that either some $NO_2^\bullet$ undergo thermally activated reaction with the parent cation

$$NO_2^\bullet + Q_2H^+ \rightarrow Q_2{}^+N(O^\bullet)OH \quad (35)$$

or, more likely, $Q_2(NO_2)^\bullet$ generated via reaction 31 is protonated, unlike other $Q_2R^\bullet$, at the oxygen rather than the C(2) atom.

$$Q_2(NO_2)^\bullet + H^+ \rightleftharpoons Q_2{}^+N(O^\bullet)OH \quad (36)$$

DFT calculations indicate that C(2)-substituted $Q_2H(NO_2)^{\bullet+}$ and $Q_2H(ONO)^{\bullet+}$ adducts would dissociate at the C(2)-heteroatom bond; i.e., in the gas phase $Q_2{}^+N(O^\bullet)OH$ is the only bound product of reaction 35.

4.3. Product Analyses. To complement these EPR studies, we carried out product analyses of irradiated room-temperature neat C_4mim NO_3 (sample 1) and the IL phase of hydrophobic C_8mim NO_3 equilibrated with 3 M DNO_3 in D_2O for 2 h immediately before the 3 MeV electron radiolysis (sample 2). In the results presented below, sample 1 was irradiated to 1.3 MGy and sample 2 was irradiated to 2.3 MGy. In our previous study,[16] we demonstrated that radiolysis of $C_n$mim TfO and $C_n$mim NTf_2 liquids yields (according to our $MS_1{}^+$ and ^1H and ^{13}C NMR spectra) mainly alkyl-substituted imidazolium cations (most likely, this substitution occurs at carbons-2, -4, and -5 in the imidazolium ring) and an assortment of oligomer cations with m/z ranging to 1500 and the mean m/z of 600 (note that mass spectra are biased to the observation of the ions and cluster ions already present in the ionic liquid, as opposed to neutral products ionized by electrospraying). Our mass spectrometry and NMR results were consistent with C−C dissociation in the long arm of the cations and the subsequent attachment of the released (fragment) $R^\bullet$ and $Q_1R^{\bullet+}$ to the imidazolium ring of the parent cations or the oligomer polycation, reactions 37 (for X = R)

$$Q_1R^{\bullet+} + Q_2H^{\bullet+} \rightarrow Q_2H(RQ_1)^{\bullet2+} \quad (37)$$

The resulting dimeric dications associated with the parent anions are observed in the mass spectra exhibiting the characteristic m/z 14−15 "period" originating from the C−C cleavage in the long arm of the parent cation occurring at different positions (Figure 24S). Such oligomerization reactions are likely to be radical reactions: for neutral aromatic molecules, the derivatization of

the aromatic ring can occur either through Friedel−Crafts chemistry (addition of carbonium ions) or radical addition; for imidazolium cations, only radical addition is possible.

It must be noted that the conditions for oligomerization due to radical−radical reactions such as reaction 37 are most favorable under high-dose-rate radiolysis, which is the case for the electron beam irradiations done here. Although reaction 37 and other radical−radical reactions may always occur within radiation track ends where local radical concentrations are high, their importance as homogeneous second-order reactions is greatly reduced under the conditions of low-dose-rate radiolysis and radiation exposure during spent fuel recycling processes.

Some amount of alkyl-substituted Q_mR^+ cations (m = 2, 4, 5) can be found in all imidazolium ILs as trace impurities in the IL before radiolysis (Figures 25S and 26S), due to synthesis byproducts. Similarly, the MS_1^+ spectra of samples 1 and 2 indicated that -NO, and -NO_2 substitution of the parent cations occurred (to a small degree, 0.1−0.5%) before radiolysis. The yield of such products is low (<1%), but so was the yield of radiation-driven substitution, increasing the concentration of such derivatives. The only type of substitution in radiolyzed samples that did not occur as a thermal reaction was -OH substitution (Figures 25S and 26S). The MS_1^+ spectra of irradiated sample 1 indicate the formation of ions such as $Q_mR^{\bullet+}$ (Figure 26S); in addition, there are many peaks with m/z between 200 and 500, which correspond to oligomer cations. The distribution of these oligomer cations has a maximum around m/z 250, as opposed to m/z 500−1000 for $C_n$mim TfO and $C_n$mim NTf_2. The narrowing of the distribution and the lower mass of the cations can be in part explained by the lower mass of the anions associated with the oligomer polycations and in part explained by inhibition of the oligomer growth by the release of $NO_2^\bullet$ during the radiolysis, as these radicals recombine with the $R^\bullet$ and $Q_1R^{\bullet+}$, arresting the growth of the oligomers. This inhibition is also suggested by the fact that the mass spectra exhibit a well-resolved m/z 14 progression. In sample 1, these oligomers account for ∼20% of the total ion counts; in sample 2, this fraction is ∼30%; i.e., the oligomerization is very extensive at these high doses. The MS_1^- spectra of sample 1 (Figure 27S) are dominated by the $C_m(NO_3)_{m+1}^-$ (m = 1−8) anions (where C^+ is the parent cation) with the smaller −19 and −62 satellites suggesting that such clusters can eliminate hydronium and nitrate. Our mass spectrometer did not operate in the low mass range, so we could not detect the NO_x^- anions directly using this technique. However, ^{14}N NMR spectra of the irradiated C_4mim NO_3 obtained in D_2O (Figure 28S) indicate ∼5.5% conversion of nitrate to nitrite; the formation of nitrite in the radiolysis of nitrate ILs has also been reported by other researchers.[22]

In the ^{1}H NMR spectra of the irradiated sample 1, there are additional resonance lines that are not observed before radiolysis (Figure 29S). Normalizing to the parent compound by integration, there are 0.5 H peaks between 1.5 and 2 ppm (Figure 29S, panel a), 1.8 H peaks between 2.3 and 4 ppm (Figure 29S, panel b), 0.16 H peaks between 6 and 7 ppm, and 0.14 H peaks between 7.8 and 9 ppm (between the resonance lines of H_2 and $H_{4,5}$ protons). Only some of these lines can be attributed. For example, the doublet of doublets at 7 ppm is certainly from the $H_{4,5}$ protons in C(2)-substituted imidazolium cations, suggesting that such substitution accounts for 4% of the products. The 6.2 ppm singlet is from decoupled H_4 or H_5 protons, indicating the substitution at C(4) and C(5) in addition to the substitution at C(2). The singlets observed between 8 and 9.5 ppm are probably from the fragment and oligomer species substituted at C(4,5) (Figure 29S, panel c); the yield of such (di) substitution can be as high as 14%. The singlets observed between 3.7 and 4 ppm are from the >C(m)−Me protons (m = 2, 4, 5); such products account for about 12% of the radiolytic products derived from the imidazolium cations. The multiplets observed at 1.5−1.8 ppm indicate the formation of new types of methylene protons in the (substituting) alkyl groups and the "tail" at 0.8−0.9 ppm indicates new types of terminal methyl groups in the aliphatic chains. These ^{1}H NMR spectra support our interpretation of MS_1^+ spectra. Poor spectral resolution in ^{1}H NMR spectra of C_8mim NTf_2:DNO_3 samples (Figure 30S) precludes attributions, but the (additional) lines fall into the same spectral regions.

Scheme 2. Radiolytically-Induced Fragmentation of HDMP in Ionic Liquids[a]

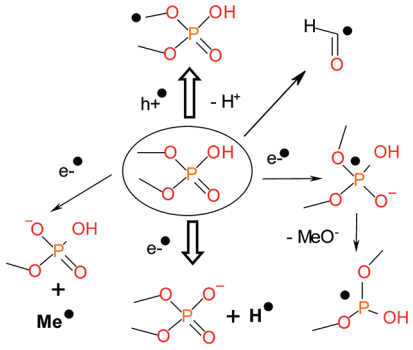

[a] The major reactions are indicated with block arrows.

The overall conclusion is that despite the dramatic change in radiation chemistry caused by the presence of nitrate and nitric acid in the imidazolium ILs, and some -OH, -NO, and -NO_2 derivatization of parent cations, the damage patterns of the imidazolium ions in nitrate-containing ILs qualitatively remain similar to other imidazolium ILs. As suggested by our EPR results, the nitrate is mainly involved in the *reductive* pathway that leads to the formation of relatively unreactive $NO_2^\bullet$ radicals. The yield of other nitrate-derived radicals is low, and these (more reactive) radicals tend to attack the most abundant species in the reaction mixture, that is, the parent cation, and thus not contributing to the oligomerization.

4.4. Dialkylphosphoric Acids. *4.4.1. Model System: Dimethylphosphoric Acid.* Radiolysis of neat frozen liquid dimethylphosphoric acid (HDMP) produced several radicals (Figure 31S, panel a); the most prominent of these radicals is $^\bullet CH_2OP(OH)_2OMe$ (Scheme 2) which accounts for most of the EPR signal; superimposed on the triplet of this radical is a quartet of narrow lines from methyl radical (which accounts for 5% of the total signal, by double integration). Subtracting these lines yields the broad triplet of $^\bullet CH_2O\sim$. The methyl radical slowly decays (10 h) at 77 K, and the residual spectrum is again from the same radical. We were also able to produce this radical by photooxidation of aqueous HDMP and trimethylphosphate on anatase nanoparticles irradiated at 355 nm; the resulting spectrum is superimposed on the EPR spectra from irradiated neat HDMP in Figure 31S(a). Interestingly, this TiO_2 photooxidation also produced a weak low-field line from the formyl radical; both resonance lines of this radical are observed in irradiated neat HDMP (Figure 31S(b)). This TiO_2 photooxidation experiment identifies $H^\bullet CO$ and $^\bullet CH_2O\sim$ as the products of HDMP *oxidation*, which accords with reactions 29 suggested in section

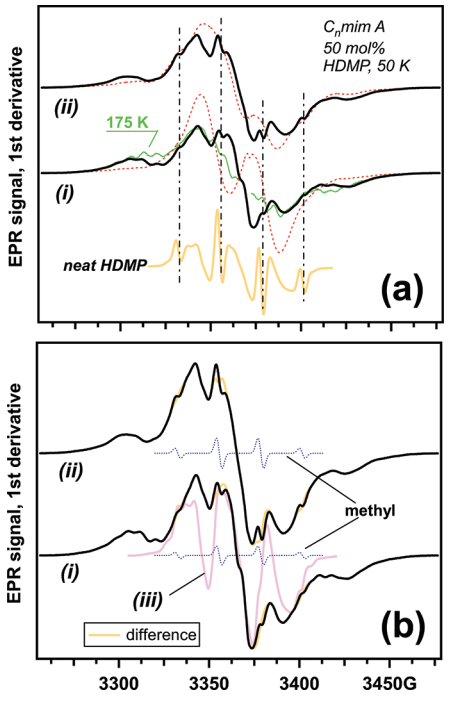

Figure 5. (a) First derivative EPR spectra from irradiated frozen solutions of (i) C_4mim PF_6 and (ii) C_5mim NTf_2 containing 50 mol % dimethylphosphoric acid (HDMP) obtained at 50 K. The dashed lines are EPR spectra from irradiated neat ILs; in i, the EPR spectrum obtained from a sample warmed to 175 K is also shown. The spectra were normalized by their double integrals. Shown below is the spectrum from irradiated neat HDMP; the vertical lines indicate the position of the quartet of the lines from methyl radical (the rest of the EPR signal is from $^{\bullet}CH_2OP\sim$). The wings in traces i and ii are from the corresponding $Q_2H_2^{\bullet+}$, showing a partially (and, in the 175 K trace, fully) resolved 7 G pattern. (b) Decomposition of traces i and ii illustrating the contributions from the methyl and $^{\bullet}CH_2OP\sim$ radicals.

2.3; warming of the sample to 150 K (Figure 32S) yields the fully resolved doublet feature which is clearly from ^{31}P splitting, and the spectrum is very similar to that observed from γ-irradiated $MeOPO_3Na$ (see Figure 1b in ref 50) that Nelson et al.[50] attributed to $^{\bullet}CH_2OPO_3^-$ with $a(2H)$ = 18.6 G and $a(^{31}P)$ = 5.7 G (vs our estimates of $a(2H)$ = 20.8 G and $a(^{31}P)$ = 4.9 G). Reaction of the hydroxyl radical with trimethylphosphate is known to produce a similar radical with $a(2H)$ = 20.1 G and $a(^{31}P)$ = 10.3 G.[50,51]

Closer examination of the EPR spectrum at a higher gain and broader field sweep reveals the signal from a ^{31}P-centered radical shown in Figures 31S(a)and 32S(b). Once again, this EPR signal is similar to the one observed by Nelson et al.[50] in irradiated $(MeO)_2PO_2Na$ and attributed by these workers to the superposition of the resonance lines from the phosphoryl ($MeOP^{\bullet}O_2^-$) and phosphoranyl ($(MeO)_2P^{\bullet}O_2^{2-}$) (see Figure 2a,b in ref 50 and Scheme 2). The EPR signal observed in irradiated HDMP is mainly from $MeOP^{\bullet}O_2H$ (the weaker EPR signal from the phosphoranyl radical fully decays at 125 K, as shown in Figure 32S(a)); together, these P-centered radicals account for 3.5% of the total radical yield. The radicals resulting from the dealkylation of HDMP (phosphoryl, methyl, and formyl) accounted for 8−10% of the radical yield, with the rest taken by $^{\bullet}CH_2OP(O_2H)OMe$. This large disparity in the yields of radicals produced by electron and hole scavenging suggests that *most of the electron trapping in neat HDMP occurs via reaction (18)*, resulting in the formation of mobile H$^{\bullet}$ atoms that abstract hydrogen from the parent molecule, yielding the same radical product as the hole trapping reaction 28a.

HDMP is freely miscible with all imidazolium ILs, which makes it the ideal model for practically important long-chain dialkylphosphonic acids, $(RO)_2PO_2H$, such as HDBP (R = *n*-butyl) and HDEHP (R = 2-ethylhexyl) that mix only with C_{10}mim NTf_2. Figure 5a demonstrates EPR spectra obtained in radiolysis of ∼50 mol % HDMP in (i) C_4mim PF_6 (see Figure 33S for other HDMP concentrations and a wider field sweep) and (ii) C_5mim NTf_2 (see also Figure 34S). The most striking features of these spectra are strong signals from $Q_2H_2^{\bullet+}$, suggesting the same chemistry as that observed for C_4mim HSO_4, namely, generation of H$^{\bullet}$ atoms via reaction 18 involving HDMA followed by the attachment of these H atoms to the parent cation. Warming of solution i to 175 K reveals a well-resolved EPR signal from the $Q_2H_2^{\bullet+}$ radical confirming our spectral attribution (Figure 5a).

In addition to the signal from the H-atom adduct, there are discernible signals from the solute: the $^{\bullet}CH_2O\sim$ and methyl radicals (Figure 5b). The latter signals can be numerically subtracted (Figure 5b), and the contribution of the methyl radicals generated via the dealkylation to the total radical yield can be estimated: this contribution amounts to 0.17% for solution i and 0.29% for solution ii, which is roughly one-tenth of the relative methyl yield in neat HDMP (see above). Thus it appears that the presence of the IL significantly decreases electron scavenging by HDMP, leading to the dealkylation of the scavenger: most of the electrons that attach to HDMP yield H$^{\bullet}$ atoms. The yield of the phosphoryl radical is also reduced (Figures 33S(b) and 34S(b)): in system i this yield is 0.4% of the total radical yield. The comparison of the EPR spectra from solution i and that from $^{\bullet}CH_2O\sim$ suggests that the latter accounts for 37% of the total radical yield. The mole fraction of HDMP in solution i corresponds to a 31% fraction in the unpaired electron density, suggesting that the ionization of HDMP roughly scales with the mass stopping power of the solute; i.e., the excitation is direct. At intermediate concentrations of HDMP (Figure 33S(a)), the signal from $Q_2H^{\bullet}$ is also discerned, i.e., reaction 18, yielding the H$^{\bullet}$ atoms from HDMP, which competes with reaction 17 and yields the 2-imidazolyl radical from the parent cation. Figure 35S demonstrates the comparison of EPR spectra from solutions containing HDMP in C_4mim-h_3 PF_6 and C_4mim-d_3 PF_6 (that is, the H(2,4,5) deutero trisubstituted cation). Due to the deutero substitution, the spectra of $Q_2HD^{\bullet+}$ and $Q_2D^{\bullet}$ become narrower, and the overlap with the methyl radical is reduced. It is seen from these spectra that the relative yield of the methyl radical does not significantly change with increasing concentration of HDMP, suggesting that some methyl radicals react with HDMP to produce secondary $^{\bullet}CH_2O\sim$, reducing the apparent yield of the dealkylation. However, even with this reaction taken into account, the dealkylation yield must be well below 1% of the total radical yield; the main chemical pathway is clearly reaction 18. The yield of the phosphoryl radical is also very low, and it scales approximately linearly with the mole fraction of the HDMP.

4.4.2. Long-Chain Dialkylphsophoric Acids. For long-chain dialkylphosphonic acids, HDEHP and HDBP (that are used for Ln^{3+} separations),[26,27] the identification of the radicals is complicated by the fact that C-centered radicals in the aliphatic tails of these molecules cannot be readily differentiated from $Q_1R^{\bullet+}$ in the long arms of $C_n$mim$^+$ (while these acids are only soluble in C_{10}mim NTf_2). Irradiation of neat HDEHP and HDBP produces the EPR spectra shown in Figure 36S. The main contribution to these spectra is from the $\sim CH_2C^{\bullet}HOP\sim$ radicals generated by

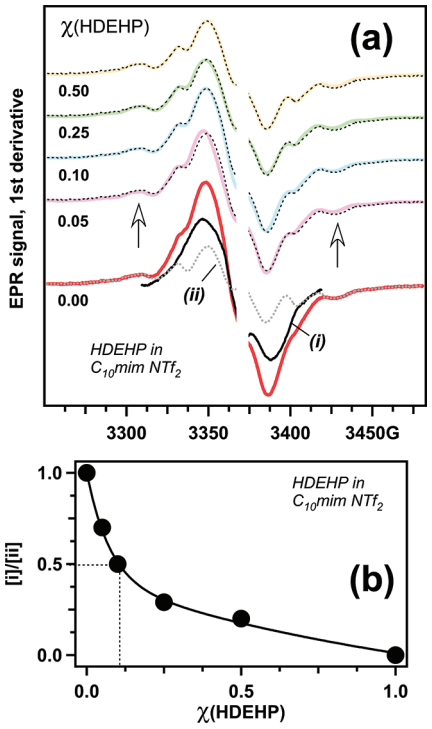

Figure 6. (a) As in Figure 3a, for C_{10}mim NTf_2 containing HDEHP. The trace for C_{10}mim NTf_2 is decomposed into the signals from (i) $(Q_2H)_2^{\bullet+}$ and (ii) "alkyl" radicals (see Figure 7). (b) Ratio of these two signals plotted as a function of the mole fraction of HDMP. The solid line is a guide for the eye.

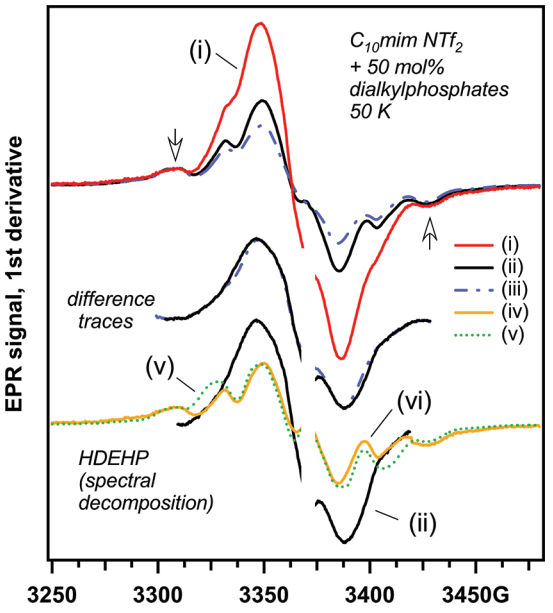

Figure 7. Top: EPR spectra from irradiated neat C_{10}mim NTf_2 (trace i) and the same liquid containing 50 mol % HDEHP (trace ii) and HDBP (trace iii). These EPR spectra were normalized by their side lines, as indicated in the plot. Middle section: traces ii and iii subtracted from trace i. Bottom: Trace i decomposed into the difference trace from the middle and trace iv which is compared to trace v from irradiated neat HDEHP.

oxidation of the parent molecules, with other *C*-centered radicals superimposed on the EPR signal from this radical. Observe that the $a(^{31}P)$ constant for such radicals is ~45 G as opposed to 4−10 G in $^{\bullet}CH_2OP\sim$, as the hfcc for phosphorus rapidly increases with an increase in the $H_\alpha COP$ dihedral angle, as noted in ref 51 and illustrated in the DFT calculation shown in Figure 37S. The phosphoranyl radical is not observed, and alkyl fragment radicals, even if they are generated, cannot be spectrally distinguished from these other C--centered radicals.

Figure 6a exhibits the EPR spectra of C_{10}mim NTf_2 containing 0−50 mol % HDEHP and HDBP. We have normalized these spectra in the "wings" (indicated by arrows), where the EPR signal is mainly from C-centered radicals. With such normalization, the main effect of the addition of the acid is a progressive decrease in the intensity of the central peak (see also Figure 38S). In Figure 7, we subtract the normalized EPR spectra obtained from 50 mol % solutions of HDEHP and HDBP in C_{10}mim NTf_2 (traces ii and iii) from the normalized EPR spectrum from neat IL (trace ii); it is seen that for both solutes the "disappearing" EPR signal is the same; it is the spectrum that we previously attributed to $(Q_2H)_2^{\bullet+}$, the product of the cation reduction. Thus, qualitatively, the effect of the HDEHP and HDBP addition is the same as that of acid addition in general: competitive electron scavenging with the formation of $H^{\bullet}$ atoms that reduces the yield of the cation reduction. The difference from HDMP is that the released $H^{\bullet}$ atoms have (statistically) much greater probability to abstract hydrogen from the long aliphatic chains of the $C_n$mim$^+$ cation and/or the dialkylphosphoric acid solute (forming a C-centered alkyl radical) than to add to the imidazolium ring. Consequently, the prompt yield of $Q_2H_2^{\bullet+}$ is low. In Figure 7, using the difference trace obtained as stipulated above, we decomposed the EPR spectrum observed in neat C_{10}mim NTf_2 into the contributions from the $(Q_2H)_2^{\bullet+}$ and (mainly) $Q_1R^{\bullet+}$ radicals (the residual EPR signal shown in trace iv); it is seen that the latter EPR spectrum is very similar to the EPR spectrum of alkyl radicals generated in radiolysis of neat HDEHP (trace v in the same plot). It can be demonstrated, by integration, that these two species provide equal contribution to the total radical yield. Using these two reference spectra, in Figure 6a we represented the spectra observed at intermediate concentrations of HDEHP as weighted sums (indicated by dashed lines) of the two contributions (traces i and ii), and in Figure 6b we plot the relative fraction of $(Q_2H)_2^{\bullet+}$ (that is, i) over the overall fraction of the alkyl radicals (derived both from the C_{10}mim$^+$ and HDEHP, that is ii). As seen from Figure 6b, the HDEHP scavenges 50% of the electrons when the mole fraction of HDEHP is ~10 mol %; i.e., HDEHP is a very efficient electron scavenger albeit it less efficient than nitrate (Figure 3b). Generalizing from the results for HDMP, we expect that the main electron-scavenging reaction is H-atom formation reaction 18 as opposed to the dealkylation.

5. DISCUSSION

The primary reactions of NO_3^- (and/or HNO_3) in imidazolium ILs are shown in Scheme 3. The main reaction pathway is reductive: the nitrate and nitric acid serve as efficient electron scavengers yielding either $NO_3^{\bullet 2-}$ or $NO_2^{\bullet}$. In the presence of water (or acids), only the latter radical is generated. $NO_3^{\bullet 2-}$ convert to $NO_2^{\bullet}$ by hydrolysis and/or protonation; our data also hint that the protonation of $NO_3^{\bullet 2-}$ might involve the parent cation (reaction 31) yielding $Q_2(NO_2)^{\bullet}$. Our DFT calculations for 1,2-dimethylimidazolium derivative (Table 2S and Figure 1S) suggest that unlike in other $Q_2X^{\bullet}$ (σ-)radicals, carbon-2 in this

dx.doi.org/10.1021/jp206579j |*J. Phys. Chem. B* 2011, 115, 10927–10942

Scheme 3. Reactions of the Nitrate Anion in Radiolysis of Imidazolium Ionic Liquids[a]

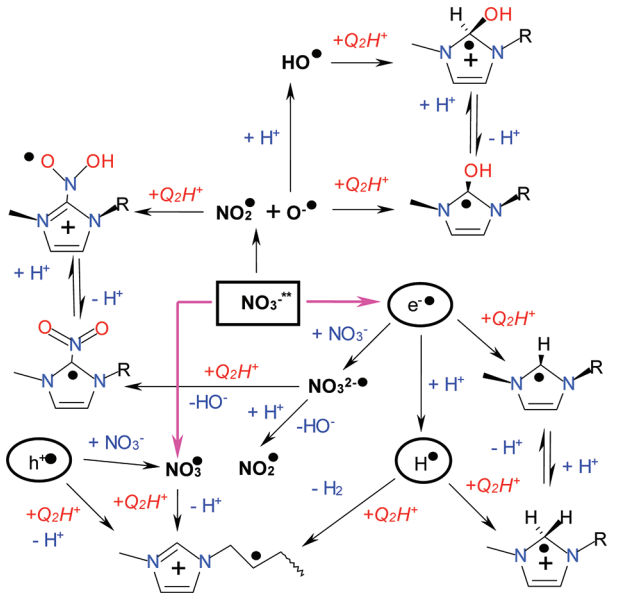

[a] The most important reactions follow the electron-reduction pathway leading to $NO_2^{\bullet}$ radical.

C_{2v}-symmetric $Q_2(NO_2)^{\bullet}$ p-radical is planar, with the nitro group in the plane of the imidazolium ring. The radical whose nitro group is in the symmetry plane perpendicular to the plane of the imidazolium ring dissociates to $^3Q_2^{\bullet\bullet} + NO_2^{\bullet}$. According to these calculations, the C(2)-protonated form of this radical is also unstable (dissociating to $Q_2H^+ + NO_2^{\bullet}$); however, the protonation in the nitro group yields a stable hydroxynitroxide radical, $Q_2{}^+N(O^{\bullet})OH$, which we believe was observed in irradiated nitrate-doped samples warmed to 200 K. The latter radical might also be produced via the direct reaction between $NO_2^{\bullet}$ and Q_2H^+ at these higher temperatures. In terms of the electronic structure, the resulting $Q_2(NO_2)^{\bullet}$ radical is closer to nitroaromatic radical anions ($ArNO_2^{\bullet-}$) than other $Q_2X^{\bullet}$ radicals. For the nitroaromatic radical anions, a protonation equilibrium analogous to reaction 36 is well-known in electrochemistry,[57] and the reactions of the resulting (neutral) $ArN(O^{\bullet})OH$ radicals have been studied in great detail. The two major reactions of these $ArN(O^{\bullet})OH$ radicals are disproportionation to $ArNO_2$ and $ArN(OH)_2$ or electron transfer from the parent radical anion to yield $ArNO_2$ and $ArN(O^-)(OH)$; the latter species is protonated to yield $ArN(OH)_2$ that in turn decomposes to ArNO + H_2O. In analogy to this chemistry, the hydroxynitroxide $Q_2{}^+N(O^{\bullet})OH$ is likely to convert to nitro and nitroso derivatives of the parent cation, that is $Q_2{}^+(NO_2)$ and $Q_2{}^+(NO)$. $Q_2{}^+(NO_2)$ can also be generated via the charge recombination involving the $Q_2(NO_2)^{\bullet}$ species. Because $NO_2^{\bullet}$ is a strong electron acceptor, the recombination can produce the nitrite anion (identified as one of the main radiolytic products) and, in the acidic IL solutions, nitrous acid. Alternatively, $NO_2^{\bullet}$ can dimerize, producing N_2O_4, which either evolves or (in the presence of water and acids) hydrolyzes to NO_3^- and NO_2^- or the corresponding acids. $NO_2^{\bullet}$ will also recombine with certain organic radicals (such as $Q_1R^{\bullet+}$) to produce the corresponding nitroalkane derivatives. The nitroso derivatives can also be formed. In addition to the reactions of $Q_2(NO_2)^{\bullet}$ examined above, such derivatives can be generated via the dissociation of nitrous acid to $NO^{\bullet}$ and $NO_2^{\bullet}$ via reaction 8 followed by the recombination of these small radicals with the organic radicals present in the system. There is every reason to believe that the secondary chemistry initiated by the radiolysis of the NO_3^-/HNO_3 containing ILs is as rich and complex as this chemistry in the aqueous solutions (section 2.1); here we only focus on the primary steps of the vast reaction cascade.

In the context of Scheme 3, we see that, in addition to these reductive chemistry pathways, there is also direct excitation of the nitrate (nitric acid) that involves N−O bond dissociation to produce $NO_2^{\bullet} + O^{\bullet-}$ (or $HO^{\bullet}$); the latter radical yields $Q_2(OH)^{\bullet}$ and its protonated form, $Q_2H(OH)^{\bullet+}$ (reactions 23). This σ-radical is analogous to other $Q_2X^{\bullet}$; the adduct radical, however, has much smaller hfcc constants for the H_α proton than the ∼40 G values found for C(2)-alkyl-substituted $Q_2HX^{\bullet+}$ (Table 1S and Figure 1S). Similarly reduced hfcc's were calculated for -ONO- and -ONO_2-substituted radicals. As noted in section 2.2, such -OH-substituted 2-imidazolyl and H-adduct radicals have already been observed using transient absorption spectroscopy in radiolysis of aqueous imidazolium salts;[46] the main difference is that Behar et al.[46] suggested C(4) or C(5) substitution, whereas our results suggest C(2) substitution.

The effect of nitrate on the oxidative pathway is less pronounced. The anticipated formation of $NO_3^{\bullet}$ in the direct ionization of the nitrate was not observed, suggesting that either the (autoionizing) electronically excited state $(NO_3^-)^{**}$ is quenched by the organic matrix or the resulting $NO_3^{\bullet}$, which is a very strong oxidizer, promptly reacts with the imidazolium cations. Two modes of such reaction can be envisioned: (i) H abstraction from the aliphatic tail of the cation (resulting in the formation of the $Q_1R^{\bullet+}$) and (ii) one-electron oxidation of the imidazolium cation. For neutral aromatic molecules, it is postulated that $NO_3^{\bullet}$ adds (as -ONO_2) to the substituted carbon in the π-ring and the α-hydrogen is abstracted by the free oxygen; another possibility is oxidation followed by deprotonation of the radical cation (in the case of the imidazolium, it is the radical dication). Regardless of the exact mechanism, this reaction should produce $Q_1R^{\bullet+}$. Indeed, as was shown in section 4.2.3, the yield of such radicals $Q_1R^{\bullet+}$ slightly *increased* in $C_n$mim CH_3CO_2:NO_3^- as compared to neat $C_n$mim CH_3CO_2.

This interpretation, however, contradicts the observations of Behar et al.[46] who concluded that $SO_4^{\bullet-}$ oxidizes $C_n$mim$^+$ to the radical dication (reaction 24) which is stable in aqueous solution. This contention was supported by the fact that the optical absorption spectrum for the product of oxidation of C_4mim$^+$ by the sulfate radical anion did not correspond to the spectrum of an alkyl radical. On the other hand, the absorption spectrum of the tentative $C_4mim^{\bullet 2+}$ looked remarkably similar to the absorption spectra of $Q_2H_2^{\bullet+}$ and $Q_2H(OH)^{\bullet+}$ studied by the same authors. Our EPR studies demonstrated[15,16] that alkyl radicals ($R^{\bullet}$), such as methyl and hydroxymethyl, readily attach to the parent cation, forming the corresponding $Q_2HR^{\bullet+}$ adduct. We suggest that the alkyl terminus of the $Q_1R^{\bullet+}$ radical attacks the C(2) atom of the imidazolium ring to yield the cyclical adduct shown in Scheme 4; the optimized geometry structures obtained using the DFT method are shown in Figures 8a and 39S. These calculations suggest that the internal cyclization is energetically favorable for C_γ- and C_δ-centered $Q_1R^{\bullet+}$ (Figure 8b), resulting in the formation of the five- and six-carbon rings; the corresponding adducts can deprotonate, yielding the substituted 2-imidazolyl radicals (Scheme 4). The high exothermicity of the cyclization suggests that this reaction is likely to occur once the temperature is

Scheme 4. Postulated Internal C_2-C_δ Cyclization of $Q_1R^{\bullet+}$

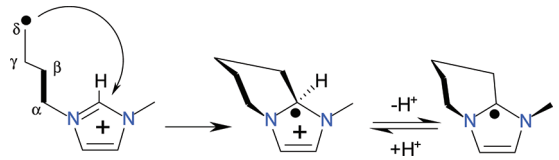

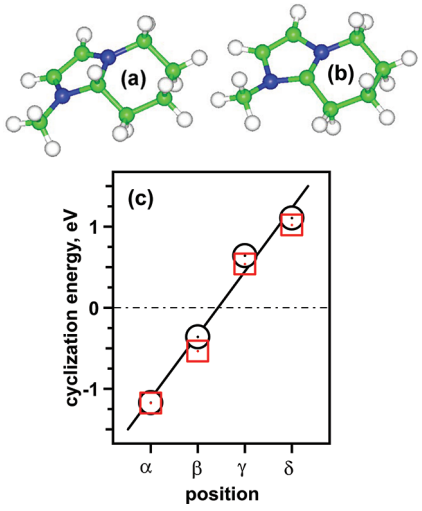

Figure 8. Geometry optimized structures for the $C_\delta-C(2)$ bound terminal $Q_1R^{\bullet+}$ derived from C_4mim^+ (a) and the corresponding deprotonated radical (b). In panel c, the cyclization energy is plotted as a function of the position of the unpaired electron in the butyl arm of $Q_1R^{\bullet+}$. The circles correspond to planar geometry of the (extended arm) $Q_1R^{\bullet+}$, whereas the squares correspond to the folded-arm geometry (with a twist at C_β, which is the lowest energy conformation).

sufficiently high to allow the conformational dynamics in the long aliphatic arm of the cation. The formation of the internal C(2) radical adduct readily accounts for the similarity of the absorption spectra from this radical and other radical adducts.

Our results indicate that as little as 3 mol % of the nitrate can compete with the parent cations as an electron scavenger, capturing 50% of the negative charge (C_{50}); the C_{50} is still lower for HNO_3. In ref 8 we demonstrated that after equilibration of C_{10}mim NTf_2 with 3 M HNO_3 (1:1 (v/v)), 0.37 and 0.16 M of NO_3^- was observed in the IL solution with and without the H_3O^+-transferring ionophore (0.1 M dicyclohexano-18-crown-6, DCH18C6). This crown ether (L) forms the 1:1:1 complex with the nitric acid, in which the three hydrogens of H_3O^+ form H-bonds with the three oxygens of the crown ring; the nitrate forms an ion pair with this $\{H_3O^+ \cdot L\}$ complex. At high concentration of HNO_3, undissociated and/or incompletely dissociated nitric acid can also form 1:1:1 and 2:2:1 complexes (HNO_3−water−crown ether) in which the water molecules are H-bound to the opposing oxygens in the crown ring and these water molecules are also bound to the oxygens of the HNO_3 molecules. These studies indicate that HNO_3 transfer to the IL phase is by neutral extraction; the exchange of the IL-constituent ions between the organic and aqueous phases is negligible. From other studies,[10] it is known that the mole fraction of the extracted HNO_3 scales approximately linearly with the acidity of the aqueous solution. These results, in the view of the data presented in section 4.2.1, suggest that the amount of nitric acid and nitrate extracted by (hydrophobic) imidazolium IL diluents from 1 to 6 M HNO_3 solutions (even without the ionophore) is fully sufficient to trap most of the electrons (which become converted to $NO_2^{\bullet}$).

6. CONCLUSION

Acids serve as exceptionally efficient electron scavengers in imidazolium ILs, despite the competition from the imidazolium cations, with a few mole percent of these acids readily outcompeting the parent cations.

For dialkylphosphonic acids (section 4.4 and Scheme 2), which are an important class of extracting agents for trivalent metal ions in nuclear separations, the main electron-trapping reaction is $H^{\bullet}$ atom formation, reaction 18. The dealkylation of the intermediate phosphoranyl radical anion (Scheme 2) through the elimination of the alkyl radical and/or alkoxide anion (as well as homolytic cleavage of the excited molecule) is greatly suppressed in imidazolium IL solutions. The released $H^{\bullet}$ atoms attach to the imidazolium ring of the parent cation or abstract H from the aliphatic tails of the cations and/or the solute; this H-abstraction becomes more prevalent for either dialkylphosphates or imidazolium cations with long aliphatic arms. The same C-centered radicals are produced by radiolytic oxidation of the IL solutions; such reactions cause damage to the solute but are not expected to result in dealkylation that interferes with the function of the extracting agent in metal ion separations. The observed yield of dealkylation is reduced ~10× in 5−50 mol % dialkylphosphoric acid solutions as compared to neat dialkylphosphoric acids. This reduction is partly due to the competitive electron scavenging (at low concentration of the solute) and partly due to the promotion of H atom elimination by efficient solvation of the released dialkylphosphate anion. The radioprotection can also be due to the quenching of the excited-state phosphoranyl radical, which is the intermediate of the dissociative electron attachment. Our results indicate that the imidazolium IL host actively "protects" the extractant/ionophore solutes from detrimental fragmentations, leading to the loss of extraction efficiency and selectivity. Of course, less damage to the solute means more damage to the solvent; however, the latter damage is less consequential for the intended application.[12]

When hydrophobic ILs are put in contact with 1−6 M nitric acid solutions, these diluents extract a sufficient amount of aqueous nitric acid to convert all of the electrons released in the radiation-induced ionization events to $NO_2^{\bullet}$. Recombination of such radicals with organic radicals generated via an oxidative pathway (that is not greatly affected by the presence of HNO_3 or NO_3^-) results in nitro-substitution. In addition to these reactions, $NO_2^{\bullet}$ are generated by direct excitation of the nitrate, with the released $O^{\bullet-}/HO^{\bullet}$ initiating their own secondary radicals (Scheme 3). The resulting chemistry is complex; some of this chemistry mirrors that which occurs in aqueous solutions; however, there are important differences. In particular, the chemistry initiated by $NO_3^{\bullet}$ is downplayed in the ILs: either this radical is not formed or it promptly oxidizes parent cations. Consequently, there are no dramatic effects on the oxidative path, and the resulting pattern of radiolytic damage to the imidazolium cations is qualitatively similar to that observed in other imidazolium ILs, with extensive alkylation and cross-linking of the cations (section 4.3).

The practical import of this study is that assessing the radiation stability of IL diluents solely through comparison of the performance of neat IL solvents before and after the irradiation of the organic phase (which is the manner in which such assessments

are presently carried out) could be misleading about the behavior of actual extraction systems in which the ILs are in contact with aqueous raffinate containing nitric acid. The presence of even relatively low amounts of extracted nitrate or nitric acid has a dramatic effect on the radiation chemistry of the IL phase (section 4.2 and Figure 3). Thus, it is necessary to go the extra step and examine the radiation chemistry of complex mixtures, as in the present study. As an example, we have revealed here that the high polarity and superior solvation properties of hydrophobic ILs result in the accommodation of a sufficient quantity of extracted nitric acid for it to scavenge the electrons released by ionizing radiation, yielding nitrogen dioxide among other products and largely diverting a significant part of the radiation chemistry of the ionic liquid.

■ ASSOCIATED CONTENT

Supporting Information. Text giving lists of abbreviations and notations and reactions 1−37, tables listing isotropic hfcc parameters and Euler values (Tables 1S and 2S), and figures showing EPR spectra, simulation of EPR spectra, estimated relative yields, temperature effects, MS_1^+ and MS_1^- spectra, and ^{14}N and ^1H NMR spectra (Figures 1S−39S). This material is available free of charge via the Internet at http://pubs.acs.org.

■ AUTHOR INFORMATION

Corresponding Author
*E-mail: shkrob@anl.gov. Tel.: (630) 252-9516.

■ ACKNOWLEDGMENT

We thank M. L. Dietz, S. Dai, H. Luo, B. Moyer, R. D. Rimmer, and J. Hatcher for stimulating discussions. The work at Argonne and Brookhaven was supported by the U.S.-DOE Office of Science, Division of Chemical Sciences, Geosciences and Biosciences under Contract Nos. DE-AC-02-06CH11357 and DE-AC02-98CH10886, respectively. The programmatic support via a DOE SISGR grant "An Integrated Basic Research Program for Advanced Nuclear Energy Separations Systems Based on Ionic Liquids" is gratefully acknowledged.

■ REFERENCES

(1) Plechkova, N. V.; Seddon, K. R. *Chem. Soc. Rev.* **2008**, *37*, 123–150. Hough, W. L.; Rogers, R. D. *Bull. Chem. Soc. Jpn.* **2007**, *80*, 2262–2269. Metlen, M. S. A.; Rogers, R. D. *Acc. Chem. Res.* **2007**, *40*, 1182–1192. Binnemans, K. *Chem. Rev.* **2007**, *107*, 2592–2614. Welton, T. *Chem. Rev.* **1999**, *99*, 2071–2083.

(2) Stepinski, D. C.; Vandegrift, G. F., III; Shkrob, I. A.; Wishart, J. F.; Kerr, K.; Dietz, M. L.; Qadah, D. T. D.; Garvey, S. L. *Ind. Eng. Chem. Res.* **2010**, *49*, 5863–5868. Dietz, M. L.; Stepinski, D. C. *Talanta* **2008**, *75*, 598–603. Dietz, M. L. *Sep. Sci. Technol.* **2006**, *41*, 2047–2063. Dietz, M. L.; Stepinski, D. C. *Green Chem.* **2005**, *7*, 747–750. Dietz, M. L.; Dzielawa, J. A.; Laszak, I.; Young, B. A.; Jensen, M. P. *Green Chem.* **2003**, *5*, 682–685. Jensen, M. P.; Neuefeind, J.; Beitz, J. V.; Skanthakumar, S.; Soderholm, L. *J. Am. Chem. Soc.* **2003**, *125*, 15466–15473. Dietz, M. L.; Dzielawa, J. A. *Chem. Commun. (Cambridge, U. K.)* **2001**, 2124–2125.

(3) Luo, H.; Dai, S.; Bonnesen, P. V.; Haverlock, T. J.; Moyer, B. A.; Buchanan, A. C., III. *Solvent Extr. Ion Exch.* **2006**, *24*, 19–31. Luo, H.; Dai, S.; Bonnesen, P. V. *Anal. Chem.* **2004**, *76*, 2773–2779. Dai, S.; Ju, Y. H.; Barnes, C. E. *J. Chem. Soc., Dalton Commun.* **1999**, 1201–1202. Luo, H.; Dai, S.; Bonnesen, P. V.; Bychanan, A. C., III. *J. Alloys Compd.* **2006**, *418*, 195–199. Chen, P. Y.; Hussey, C. L. *Electrochim. Acta* **2004**, *49*, 5125–5138.

(4) Cocalia, V. A.; Gutowski, K. E.; Rogers, R. D. *Coord. Chem. Rev.* **2006**, *250*, 755–764. Ouadi, A.; Klimchuk, O.; Gaillard, C.; Billard, I. *Green Chem.* **2007**, *9*, 1160–1162.

(5) Dietz, M. L.; Dzielawa, J. A.; Jensen, M. P.; Beitz, J. V.; Borkowski, M. *Ionic Liquids IIIB: Fundamentals, Progress, Challenges and Opportunities: Transformations and Processes*; American Chemical Society: Washington, DC, 2005; Vol. 902, pp 2−18; Gaillard, C.; Moutiers, G.; Mariet, C.; Antoun, T.; Gadenne, B.; Hesemann, P.; Moreau, J. J. E.; Ouadi, A.; Labet, A.; Billard, I. *Ionic Liquids IIIB: Fundamentals, Progress, Challenges and Opportunities: Transformations and Processes*, American Chemical Society: Washington, DC, 2005; Vol. 902, pp 19−32.

(6) Nash, K. L. In *Separations for the Nuclear Fuel Cycle in the 21st Century*; Lumetta, G. J., Nash, K. L., Clark, S. B., Friese, J. I., Eds.; American Chemical Society: Washington, DC, 2006; Vol. 933, pp 21−40; Billard, I.; Ouadi, A.; Gaillard, C. *Anal. Bioanal. Chem.* **2011**, *400*, 1555–1566.

(7) Shkrob, I. A.; Marin, T. W.; Dietz, M. L. *J. Phys. Chem. B* **2011**, *115*, 3903–3911.

(8) Marin, T. W.; Shkrob, I. A.; Dietz, M. L. *J. Phys. Chem B* **2011**, *115*, 3912–3918.

(9) Berthon, L.; Chabronnel, M.-C. In *Ion Exchange and Solvent Extraction, A Series of Advances, Vol.* 19; Moyer, B. A, Ed.; CRC Press: Boca Raton, FL, 2010; pp 429−513.

(10) Giridhar, P.; Venkatesan, K. A.; Srinivasan, T. G.; Rao, P. R. V. *J. Nucl. Radiochem. Sci.* **2004**, *5*, 21–26. Giridhar, P.; Venkatesan, K. A.; Srinivasan, T. G.; Rao, P. R. V. *J. Radioanal. Nucl. Chem.* **2005**, *265*, 31–38. Venkatesan, K. A.; Srinivasan, T. G.; Rao, P. R. V. *J. Nucl. Radiochem. Sci.* **2009**, *10*, R1–R6. Giridhar, P.; Venkatesan, K. A.; Subramaniam, S.; Srinivasan, T. G.; Rao, P. R. V. *J. Alloys Compd.* **2008**, *448*, 104–108.

(11) Cammarata, L.; Kazarian, S. G.; Salter, P. A.; Welton, T. *Phys. Chem. Chem. Phys.* **2001**, *3*, 5192–5200.

(12) Shkrob, I. A.; Chemerisov, S. D.; Wishart, J. F. *J. Phys. Chem. B* **2007**, *111*, 11786–11793.

(13) Shkrob, I. A.; Wishart, J. F. *J. Phys. Chem. B* **2009**, *113*, 5582–5592.

(14) Shkrob, I. A. *J. Phys. Chem. B* **2010**, *114*, 368–375.

(15) Shkrob, I. A.; Marin, T. W.; Chemerisov, S. D.; Wishart, J. F. *J. Phys. Chem. B* **2011**, *115*, 3872–3888.

(16) Shkrob, I. A.; Marin, T. W.; Chemerisov, S. D.; Hatcher, J.; Wishart, J. F. *J. Phys. Chem. B* **2011**, *115*, 3889–3902.

(17) Wishart, J. F. *J. Phys. Chem. Lett.* **2010**, *1*, 3225–3231.

(18) Wishart, J. F.; Shkrob, I. A. In *Ionic Liquids: From Knowledge to Application*, Rogers, R. D., Plechkova, N. V., Seddon, K. R., Eds.; American Chemical Society: Washington, DC, 2009; pp 119−134.

(19) Wishart, J. F. *Free Radical Chemistry in Room-Temperature Ionic Liquids* In *Handbook of Radical Chemistry and Biology*; Chatgilialoglu, C., Studer, A., Eds.; Wiley: Chichester, U.K., in press.

(20) Wishart, J. F. *Energy Environ. Sci.* **2009**, *2*, 956–961. Wishart, J. F.; Neta, P. *J. Phys. Chem. B* **2003**, *107*, 7261–7267.Funston, A. M.; Wishart, J. F. In *Ionic Liquids IIIA: Fundamentals, Progress, Challenges, and Opportunities, Properties and Structure*; Rogers, R. D., Seddon, K. R., Eds.; American Chemical Society: Washington, DC, 2005; Vol. 901, pp 102−116.

(21) Yuan, L. Y.; Peng, J.; Zhai, M. L.; Li, J. Q.; Wei, G. S. *Radiat. Phys. Chem.* **2009**, *78*, 737–739.

(22) Allen, D.; Baston, G.; Bradley, A. E.; Gorman, T.; Haile, A.; Hamblett, I.; Hatter, J. E.; Healey, M. J. F.; Hodgson, B.; Lewin, R.; Lovell, K. V.; et al. *Green Chem.* **2002**, *4*, 152–158.

(23) Yuan, L. Y.; Peng, J.; Xu, L.; Zhai, M. L.; Li, J. Q.; Wei, G. S. *J. Phys. Chem. B* **2009**, *113*, 8948–8952. Qi, M.; Wu, G.; Chen, S.; Liu, Y. *Radiat. Res.* **2007**, *167*, 508–514. Yuan, L. Y.; Peng, J.; Xu, L.; Zhai, M. L.; Li, J. Q.; Wei, G. S. *Dalton Trans.* **2008**, 6358–6360. Yuan, L. Y.; Xu, C.; Peng, J.; Xu, L.; Zhai, M. L.; Li, J. Q.; Wei, G. S.; Shen, X. H. *Dalton Trans.* **2009**, 7873–7875.

(24) Berthon, L.; Nikitenko, S. I.; Bisel, I.; Berthon, C.; Faucon, M.; Saucerotte, B.; Zorz, N.; Moisy, P. *Dalton Trans.* **2006**, 2526–2534.

(25) Bosse, E.; Berthon, L.; Zorz, N.; Monget, J.; Berthon, C.; Bisel, I.; Legand, S.; Moisy, P. *Dalton Trans.* **2008**, 924–931.
(26) Le Rouzo, G.; Lamouroux, C.; Dauvois, V.; Dannoux, A.; Legand, S.; Durand, D.; Moisy, P.; Moutiers, G. *Dalton Trans.* **2009**, 6175–6184.
(27) Gannaz, B.; Chiarizia, R.; Antonio, M. R.; Hill, C.; Cote, G. *Solvent Extr. Ion Exch.* **2007**, *25*, 313–337.Hill, C. In *Ion Exchange and Solvent Extraction, A Series of Advances*, Vol. 19; Moyer, B. A., Ed.; CRC Press: Boca Raton, FL, 2010; p 170.
(28) Nilsson, M.; Nash, K. L. *Solvent Extr. Ion Exch.* **2007**, *25*, 665–701. Tachimori, S.; Nakamura, H. *J. Radioanal. Chem.* **1979**, *52*, 343–354. Gelis, A. V.; Vandegrift, G. F.; Bakel, A.; Bowers, D. L.; Hebden, A. S.; Pereira, C.; Regalbuto, M. *Radiochim. Acta* **2009**, *97*, 231–232. Leggett, C. J.; Liu, G. K.; Jensen, M. P. *Solvent Extr. Ion Exch.* **2010**, *28*, 313–334.
(29) Ha, S. H.; Menchavez, R. N.; Koo, Y.-M. *Korean J. Chem.* **2010**, *27*, 1360–1365. Cocalia, V. A.; Jensen, M. P.; Holbrey, J. D.; Spear, S. K.; Stepinski, D. C.; Rogers, R. D. *Dalton Trans.* **2005**, 1966–1971. Liu, Y.; Zhu, L.; Sun, X.; Chen, J. *AIChE J.* **2010**, *56*, 2338–2346. Rickert, P. G.; Stepinski, D. C.; Rausch, D. J.; Bergeron, R. M.; Jakab, S.; Dietz, M. L. *Talanta* **2007**, *72*, 315–320.Sun, X.; Bell, J. R.; Luo, H.; Dai, S. *Dalton Trans.* **2011**, *40*,8019−8023 (DOI: 10.1039/C1DT10873E).
(30) Katsumura, Y.; Jiang, P. Y.; Nagaishi, R.; Oishi, T.; Ishigure, K.; Yoshida, Y. *J. Phys. Chem.* **1991**, *95*, 4435–4439.
(31) Nagaishi, R. *Radiat. Phys. Chem.* **2001**, *60*, 369–375.
(32) Madsen, D.; Larsen, J.; Jensen, S. K.; Keiding, S. R.; Thogersen, J. *J. Am. Chem. Soc.* **2003**, *125*, 15571–15576.
(33) Goldstein, S.; Rabani, J. *J. Am. Chem. Soc.* **2007**, *129*, 10597–10601.
(34) Mezyk, S. P.; Bartels, D. M. *J. Phys. Chem. A* **1997**, *101*, 6233–6237.
(35) Fessenden, R. W.; Meisel, D.; Camaioni, D. M. *J. Am. Chem. Soc.* **2000**, *122*, 3773–3774. Lymar, S. V.; Schwartz, H. A.; Czapski, G. *J. Phys. Chem. A* **2002**, *106*, 7245–7250.
(36) Cook, A. R.; Dimitrijevic, N. D.; Dreyfus, B. W.; Meisel, D.; Curtiss, L. A.; Camaioni, D. M. *J. Phys. Chem. A* **2001**, *105*, 3658−3666, and references therein.
(37) Neta, P.; Huie, R. E. *J. Phys. Chem.* **1986**, *90*, 4644–4648. Umschlang, Th.; Zellner, R.; Herrmann, H. *Phys. Chem. Chem. Phys.* **2002**, *4*, 2975–2982.
(38) Rollins, A. W.; Kiendler-Scharr, A.; Fry, J. L.; Brauers, T.; Brown, S. S.; Dorn, H.-P.; Dube, W. P.; Fuchs, H.; Mensah, A.; Mentel, T. F.; et al. *Atmos. Chem. Phys.* **2009**, *9*, 6685–6703.
(39) Rindone, B.; Cariati, F.; Restelli, G.; Hjorth, J. *Fresenius' J. Anal. Chem.* **1991**, *339*, 673–675. Aschmann, S. M.; Atkinson, R. *J. Phys. Chem. A* **2011**, *115*, 1358–1363. Atkinson, R.; Aschmann, S. M.; Winer, A. M. *Eviron. Sci. Technol.* **1987**, *21*, 1123–1126.
(40) Elliot, A. J.; Simsons, A. S. *Can. J. Chem.* **1984**, *62*, 1831–1834.
(41) Ershov, B. G.; Pikaev, A. K.; Glazunov, P. Ya.; Spisyn, V. I. *Russ. Chem. Bull.* **1965**, *14*, 1891–1897.
(42) Kevan, L. *J. Phys. Chem.* **1964**, *68*, 2590–2594. *J. Phys. Chem.* **1964**, *68*, 2590–2594.
(43) Bannov, S. I.; Kriger, L. D.; Miklin, M. B. *High Energy Chem.* **2004**, *38*, 120–123. Pak, V. Kh.; Nevostruev, V. A. *High Energy Chem.* **2000**, *34*, 289–294. Padilla, J.; de Maria Ramirez, F. *J. Radioanal. Nucl. Chem.* **1999**, *242*, 653–661.
(44) Lokkevik, P.; Henriksen, T. *Radiat. Res.* **1969**, *38*, 231–247.
(45) Eda, B; Iwasaki, M. *J. Phys. Chem.* **1982**, *86*, 2084–2088.
(46) Behar, D.; Gonzalez, C.; Neta, P. *J. Phys. Chem. A* **2001**, *105*, 7607–7614.
(47) Behar, D.; Neta, P.; Schultheisz, C. *J. Phys. Chem. A* **2002**, *106*, 3139–3147.
(48) Kerr, C. M. L; Webster, K.; Williams, F. *J. Phys. Chem.* **1975**, *79*, 2650–2662. *J. Chem. Phys.* **1972**, *76*, 2848–2850.
(49) Shkrob, I. A.; Marin, T. W. *Chem. Phys. Lett.* **2008**, *465*, 234−237, and references therein.
(50) Nelson, D.; Symons, M. C. R. J. *J. Chem. Soc., Perkin Trans. 2* **1977**, 286–293.
(51) Ezra, F. S.; Bernhard, W. A. *J. Chem. Phys.* **1974**, *60*, 1711–1716. Bernhard, W. A.; Ezra, F. S. *J. Phys. Chem.* **1974**, *78*, 958–961.
(52) Kuzin, I. A.; Semuhin, A. M.; Romanovskii, V. N. *High Energy Chem.* **1969**, 3, 248–249.
(53) Kerr, C. M. L.; Webster, K.; Williams, F. *Mol. Phys.* **1973**, *25*, 1461–1464.
(54) Mincher, B. J.; Mezyk, S. P.; Martin, L. R. *J. Phys. Chem. A* **2008**, *112*, 6275–6280.
(55) Becke, A. D. *Phys. Rev. A* **1988**, *38*, 3098–3100. Lee, C.; Yang, W.; Parr, R. G. *Phys. Rev. B* **1988**, *37*, 785–789.
(56) Frisch, M. J.; Trucks, G. W.; Schlegel, H. B.; Scuseria, G. E.; Robb, M. A.; Cheeseman, J. R.; Zakrzewski, V. G.; Montgomery, J. A., Jr.; Stratmann, R. E.; Burant, J. C., et al. *Gaussian 98*, Rev. A.1; Gaussian: Pittsburgh, PA; 1998.
(57) Grimshaw, J. *Electrochemical Reactions and Mechanisms in Organic Chemistry*; Elsevier Science B. V.: Amsterdam, The Netherlands, 2000; p 372.